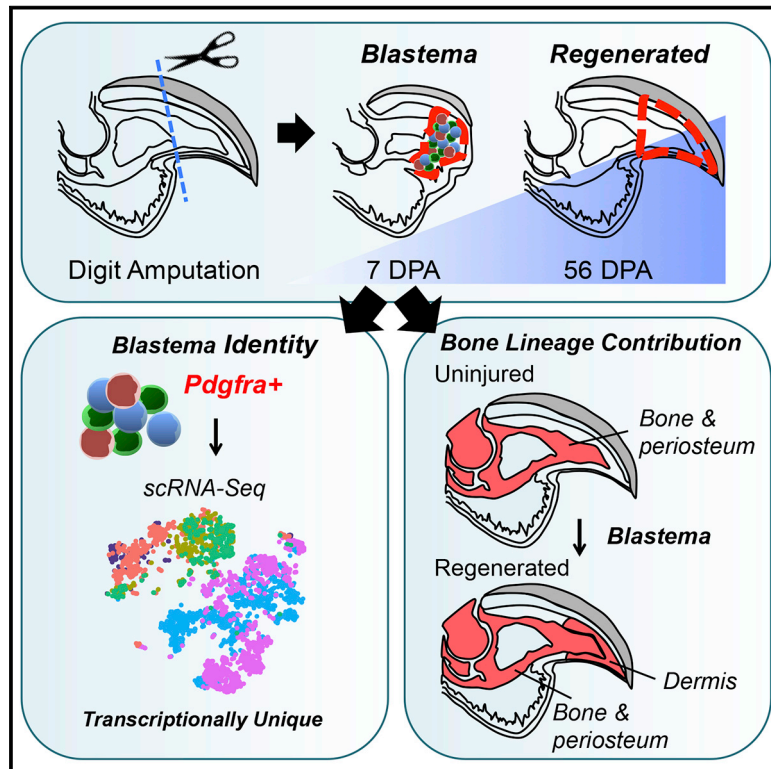


# Developmental Cell

## Acquisition of a Unique Mesenchymal Precursor-like Blastema State Underlies Successful Adult Mammalian Digit Tip Regeneration

### Graphical Abstract



### Authors

Mekayla A. Storer, Neemat Mahmud, Konstantina Karamboulas, ..., Michael V. Sefton, David R. Kaplan, Freda D. Miller

### Correspondence

fredam@sickkids.ca

### In Brief

Storer et al. use lineage tracing, single-cell RNA sequencing, and cell transplantation to define the transcriptional identity of the mesenchymal cells comprising the blastema and the major transitions during mammalian digit tip regeneration. The regenerative environment determines the adult blastema state and confers mesenchymal lineage flexibility.

### Highlights

- *Pdgfra*-expressing mesenchymal cells from uninjured digits establish the blastema
- Adult digit tip regeneration is distinct from embryonic digit development
- The blastema state is environmentally determined
- The regenerative environment enables mesenchymal lineage plasticity

# Acquisition of a Unique Mesenchymal Precursor-like Blastema State Underlies Successful Adult Mammalian Digit Tip Regeneration

Mekayla A. Storer,<sup>1,7</sup> Neemat Mahmud,<sup>1,3,7</sup> Konstantina Karamboulas,<sup>1</sup> Michael J. Borrett,<sup>1,5</sup> Scott A. Yuzwa,<sup>1,8</sup> Alexander Gont,<sup>1</sup> Alaura Androschuk,<sup>6</sup> Michael V. Sefton,<sup>4,6</sup> David R. Kaplan,<sup>1,2,5</sup> and Freda D. Miller<sup>1,2,3,5,9,\*</sup>

<sup>1</sup>Program in Neurosciences and Mental Health, Hospital for Sick Children, Toronto M5G 1L7, Canada

<sup>2</sup>Department of Molecular Genetics, University of Toronto, Toronto M5G 1A8, Canada

<sup>3</sup>Department of Physiology, University of Toronto, Toronto M5G 1A8, Canada

<sup>4</sup>Department of Chemical Engineering and Applied Chemistry, University of Toronto, Toronto M5G 1A8, Canada

<sup>5</sup>Institute of Medical Sciences, University of Toronto, Toronto M5G 1A8, Canada

<sup>6</sup>Institute of Biomaterials and Biomedical Engineering, University of Toronto, Toronto M5G 1A8, Canada

<sup>7</sup>These authors contributed equally

<sup>8</sup>Present address: Department of Laboratory Medicine and Pathobiology, University of Toronto, Toronto M5G 1A8, Canada

<sup>9</sup>Lead Contact

\*Correspondence: [fredam@sickkids.ca](mailto:fredam@sickkids.ca)

<https://doi.org/10.1016/j.devcel.2019.12.004>

## SUMMARY

Here, we investigate the origin and nature of blastema cells that regenerate the adult murine digit tip. We show that *Pdgfra*-expressing mesenchymal cells in uninjured digits establish the regenerative blastema and are essential for regeneration. Single-cell profiling shows that the mesenchymal blastema cells are distinct from both uninjured digit and embryonic limb or digit *Pdgfra*-positive cells. This unique blastema state is environmentally determined; dermal fibroblasts transplanted into the regenerative, but not non-regenerative, digit express blastema-state genes and contribute to bone regeneration. Moreover, lineage tracing with single-cell profiling indicates that endogenous osteoblasts or osteocytes acquire a blastema mesenchymal transcriptional state and contribute to both dermis and bone regeneration. Thus, mammalian digit tip regeneration occurs via a distinct adult mechanism where the regenerative environment promotes acquisition of a blastema state that enables cells from tissues such as bone to contribute to the regeneration of other mesenchymal tissues such as the dermis.

## INTRODUCTION

Some amphibians can regenerate appendages such as limbs (Brockes and Gates, 2014; Brockes and Kumar, 2002; Kragl et al., 2009; Kumar et al., 2007; Straube and Tanaka, 2006), but the capacity for multi-tissue regeneration has largely been lost in mammals. One exception to this rule is rodent and human distal digit tip regeneration, which occurs even in adults when the nail bed is intact by a multi-step process involving wound healing, epidermal closure, formation of a transient blastema, and ul-

timately tissue regeneration (Borgens, 1982; Han et al., 2008; Simkin et al., 2013; Douglas, 1972; Illingworth, 1974; Johnston et al., 2016; Fernando et al., 2011; Neufeld and Zhao, 1995).

Why then, do digit tips regenerate while other mammalian tissues do not? Experiments comparing regenerative versus non-regenerative amputations where the nail bed is removed have shown that blastema formation is the critical distinguishing event. Although the nature of the blastema is not well understood, we do know that it is largely comprised of *Pdgfra*-expressing mesenchymal cells (Johnston et al., 2016), including neural-crest-derived mesenchymal cells originating from local nerves (Carr et al., 2019). We also know that cells do not cross germline lineage boundaries during digit tip regeneration (Lehoczky et al., 2011; Rinkevich et al., 2011; Stewart and Stankunas, 2012; Tu and Johnson, 2011; Singh et al., 2012). Nonetheless, we do not know where most mesenchymal blastema cells come from, what cellular state they adopt as blastema cells, and/or whether they are flexible in terms of the mesenchymal lineages they generate. Here, we have addressed these questions using single-cell transcriptional profiling, lineage tracing, and cell transplantation and provide support for the concept that the regenerative digit tip environment promotes acquisition of a flexible precursor-like blastema transcriptional state that allows mesenchymal cells from one tissue type to contribute to regeneration of other mesenchymal tissues.

## RESULTS

### *Pdgfra*-Positive Mesenchymal Cells Generate the Blastema and Are Essential for Regeneration

We asked if the mesenchymal blastema originates from *Pdgfra*-positive cells in tissues such as bone and dermis or from *Pdgfra*-negative vasculature-associated mesenchymal cells using mice carrying *CreERT* or *CreERT2* driven by promoter or enhancer regions from the *Pdgfra* or *Myh11* genes, respectively. We crossed these to mice with an inducible *TdTomato* reporter in the *Rosa26* locus (*R26-LSL-TdT*) and treated them with tamoxifen. In uninjured adult *PdgfraCreERT;R26-LSL-TdT* mice, TdT

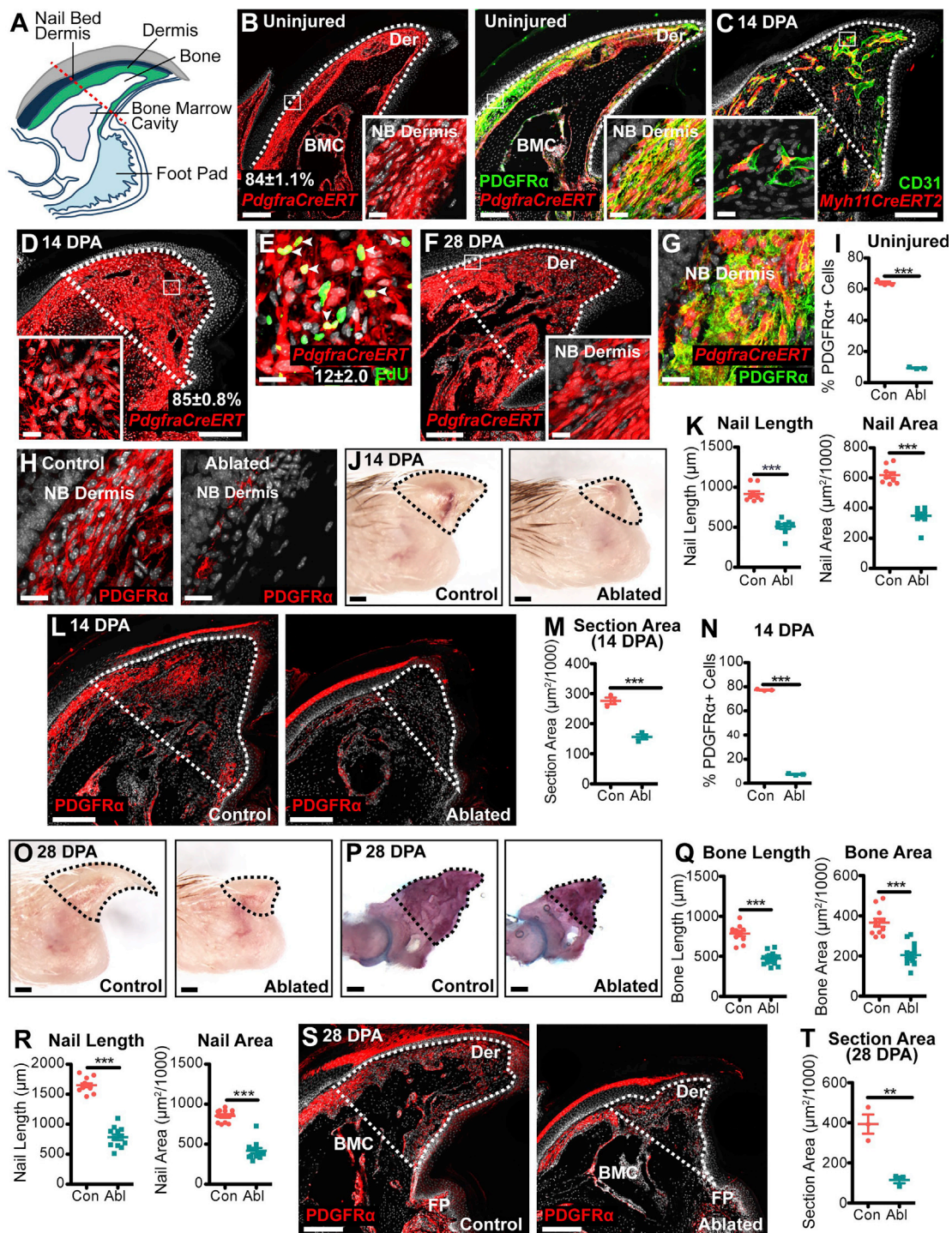


**Figure 1. *Pdgfra*-Positive Mesenchymal Cells Contribute to Blastema Formation and Digit Tip Regeneration**

(A) Digit tip schematic. Red-hatched line indicates the amputation plane.

(B) Adult *Pdgfra*CreERT;*R26-LSL-TdT* digit tip 10 days post-tamoxifen, showing TdT (red) and PDGFR $\alpha$  immunostaining (green, right). Numbers indicate percentage

of TdT-positive/total non-epithelial cells (n = 3). Insets show the boxed regions at higher magnification. Der, dermis; NB, nail bed; and BMC, bone marrow cavity.

(C) Adult *Myh11*CreERT2;*R26-LSL-TdT* 14 DPA digit tip, tamoxifen-treated 10 days prior to amputation, showing TdT (red) and CD31 immunostaining (green). Inset shows the boxed region.

(D and E) *Pdgfra*CreERT;*R26-LSL-TdT* 14 DPA digit tips from mice treated with tamoxifen prior to injury and injected with EdU at 13 DPA, showing TdT (red) and EdU immunostaining (E, green). Numbers indicate % TdT-positive/total non-epithelial cells (D) or TdT-positive cells also positive for EdU (E) (n = 6 and 3, respectively). Inset (D) shows boxed region, and arrowheads (E) denote double-labeled cells.

(legend continued on next page)

labeled 84% of non-epithelial digit tip cells, including PDGFR $\alpha$ -protein-positive cells in the dermis, bone marrow stroma, bone lining, and bone lacunae (Figures 1A, 1B, and S1A). TdT did not label p75NTR-positive Schwann cells, K14-positive epidermal cells, IBA1-positive immune cells, or CD31-positive vasculature-associated cells (Figures S1B–S1E). By contrast, in *Myh11-CreERT2;R26-LSL-TdT* mice, TdT labeled only PDGFR $\alpha$ -negative pericytes and vascular smooth muscle (VSM) cells associated with CD31-positive vasculature (Figures S1F and S1G).

To characterize regeneration in these mice, we injected them with tamoxifen, amputated digit tips 10 days later, and in some, injected 5-Ethynyl-2'-deoxyuridine (EdU) at 13 days post-amputation (DPA). At 14 DPA, the time of peak blastema activity (Simkin et al., 2013), and 28 DPA, when regenerative growth is complete, *Myh11CreERT2-TdT*-positive cells were all associated with CD31-positive vasculature and were PDGFR $\alpha$  negative (Figures 1C and S1H–S1J). By contrast, in *Pdgfra-CreERT;R26-LSL-TdT* mice at 14 DPA, almost all blastema cells were TdT positive, and 12% of these were also EdU positive (Figures 1D and 1E). By 28 DPA, TdT-positive cells were found in the dermis, bone marrow stroma, and bone matrix where they co-expressed PDGFR $\alpha$  protein and, in the dermis, THY1 (Figures 1F, 1G, S1K, and S1L). They were not associated with CD31-positive vasculature (Figure S1M).

These data indicate that *Pdgfra*-expressing cells generate the blastema. To ask if they were necessary for regeneration, we generated mice carrying *PdgfraCreERT* and an inducible active diphtheria toxin A (DTA) transgene (*R26-LSL-DTA*). Tamoxifen treatment of these mice led to the ablation of most PDGFR $\alpha$ -positive digit tip mesenchymal cells for at least 38 days (Figures 1H, 1I, S1N, and S1O). Despite this, digits were largely normal, although nail length was modestly reduced (Figures S1P and S1Q), likely because of a loss of inductive nail bed dermal cells (Takeo et al., 2013). When ablated digits were amputated, regeneration was impaired (Figures 1J–1T). At 14 DPA, the epidermis was appropriately healed, but the nail length and area, regenerated tissue area, and PDGFR $\alpha$ -positive cells were all reduced. Similar regenerative deficits were observed at 28 DPA. Thus, *Pdgfra*-positive cells are essential for the mesenchymal blastema and tissue regeneration.

### Characterizing Uninjured Digit Tip *Pdgfra*-Positive Mesenchymal Cells with Single-Cell Profiling

To characterize cells of origin for the mesenchymal blastema, we dissociated adult uninjured digit tip cells distal and immediately proximal to the amputation plane using two different protocols

that liberate all cells except tightly associated osteocytes. We sequenced 7,144 cells (see STAR Methods for details of all sequencing runs) using the 10X Genomics platform and analyzed transcriptomes using a pipeline we previously described (Yuzwa et al., 2017; Carr et al., 2019). Genes with high variance were used to compute principal components as inputs for projecting cells in two dimensions using t-distributed stochastic neighbor embedding (t-SNE), performing clustering using shared nearest neighbors-clique (SNN-clique) with a range of resolution parameters.

We combined transcriptomes from both runs (see STAR Methods) and identified 20 clusters (Figure 2A). t-SNE overlays for marker genes (Figures 2B and S2A–S2E) identified clusters containing *Pecam1/Cd31*-positive endothelial cells (3, 5, 7, and 12), *Sox10*-positive Schwann cells (19), *Aif1*-positive immune cells (14, 17, and 20), and *Krt5*-positive epidermal cells (15 and 18) as well as two groups of *Pdgfrb*-positive mesenchymal cells. One group included VSM/pericyte cells expressing *Myh11* but not *Pdgfra* (1, 2, 8, 9, and 16), and the other group included *Pdgfra*-positive cells (4, 6, 10, 11, and 13) (for further cell-type-specific marker genes used, see STAR Methods). All cell types included contributions from both preparations and sequencing runs, and this was similar with and without batch correction.

Based on the lineage tracing, we focused on *Pdgfra*-positive cells. We validated clusters 4, 11, and 13 as dermis or connective tissue (CT) cells expressing *Scara5*, *Clec3b*, and *Cd34* by performing single-molecule fluorescence in situ hybridization (FISH) and immunostaining (Figures 2C–2E and S2F–S2H). One of these clusters (13) included nail bed dermis cells, as validated by FISH for 2 highly enriched genes, *Nrg2* and *Sfrp2* (Figures 2F–2H and S2I–S2K). The other clusters included bone-lineage cells expressing osteoprogenitor genes (*Sp7/osterix*, *Wnt16*, and *Pthlh* in composite interface clusters 4 and 6) or mature osteogenic lineage genes (*Ibsp*, *Dmp1*, *Bglap*, *Spp1*, and *Mmp13* in clusters 6 and 10) (Figure 2I). Immunostaining for SP7 and FISH for *Dmp1* mRNA (Figures 2J, 2K, S2L, and S2M) confirmed these genes were limited to the bone compartment.

### Regenerating and Uninjured Digit Tip *Pdgfra*-Expressing Mesenchymal Cells Are Transcriptionally Distinct

We next profiled the regenerating digit tip, sequencing 2,090 14 DPA cells from two preparations/runs and 1,596 10 DPA cells. Analysis via the pipeline (Figures 2L–2O and S2N–S2T) defined 11 clusters at 10 DPA and 14 clusters at 14 DPA. These clusters included *Pdgfra*-positive mesenchymal cells, VSM/pericyte cells, endothelial cells, and immune cells at both time points,

(F and G) *PdgfraCreERT;R26-LSL-TdT* 28 DPA digit tips, tamoxifen treated prior to injury, showing TdT (red) and, in (G), PDGFR $\alpha$  immunostaining of the nail bed (NB) dermis. Inset (F) shows the boxed region.

(H–T) *PdgfraCreERT;R26-LSL-DTA* (ablated or Abl) or *R26-LSL-DTA* (control or Con) mice were treated with tamoxifen and some mice had digit tips amputated 10 days later. (H and I) Uninjured digit tips were immunostained for PDGFR $\alpha$  (H, red) and % PDGFR $\alpha$ -positive cells/total non-epithelial Hoechst 33258-positive cells distal to the prospective amputation plane (see A) was quantified (I) ( $n = 3$  each). (J and K) 14 DPA distal digit nails (J, hatched lines) were assessed for length and area (K) ( $n = 9$  each). (L–N) 14 DPA digit tip sections were immunostained for PDGFR $\alpha$  (red, L) and assessed for regenerated tissue area per section (M) and % PDGFR $\alpha$ -positive/total non-epithelial cells within regenerated tissue (N, outlined by hatched lines in (L)) ( $n = 3$  each). (O–R) 28 DPA distal digits (O) or bones stained with Alizarin Red and Alcian blue (P) were assessed for length and area of regenerated bones (Q) or nails (R), as outlined by hatched lines (O and P) ( $n = 11–16$  each). (S and T) 28 DPA digit tip sections were immunostained for PDGFR $\alpha$  (S, red) and regenerated non-epithelial tissue area/section was determined (T, outlined by hatched lines in (S)) ( $n = 3$  each). All images were counterstained with Hoechst 33258 (white), and (B), (C), (D), (F), (L), and (S) show stitched images. Hatched lines outline the non-epithelial uninjured digit tip or regeneration tissue. All graphs are scatterplots and error bars, SEM. \*\* $p < 0.01$ , \*\*\* $p < 0.001$ . Scale bars represent 200  $\mu\text{m}$  in (B), (C), (D), (F), (J), (L), (O), (P), and (S) and 20  $\mu\text{m}$  in (E), (G), and (H) and insets. See also Figure S1.

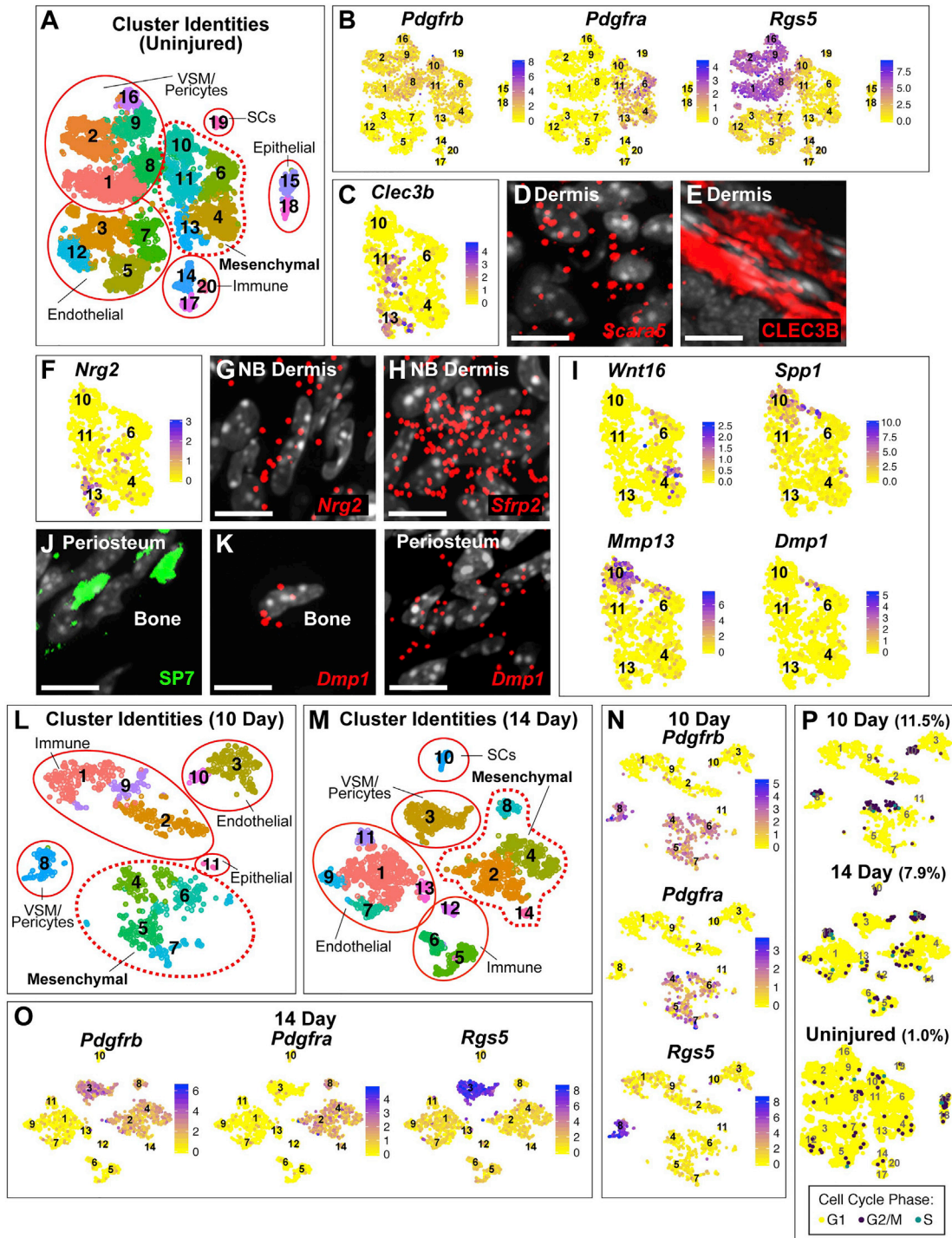


**Figure 2. Single-Cell Transcriptional Profiling to Characterize Uninjured and Regenerating *Pdgfra*-Expressing Mesenchymal Cells**

(A–C, F, and I) scRNA-seq analysis of uninjured digit tips exclusive of the nail and tightly associated osteocytes. (A) t-SNE visualization of 20 cell clusters/6 annotated cell types identified by marker genes such as the mesenchymal genes *Pdgfrb*, *Pdgfra*, and *Rgs5* (B), the dermal genes *Clec3b* and *Nrg2* (C and F) or bone lineage genes *Wnt16*, *Spp1*, *Mmp13*, and *Dmp1* (I). In (C), (F), and (I), only *Pdgfra*-positive mesenchymal clusters are shown (red hatched line in (A)).

(D and E) Uninjured digit tip sections probed by FISH for *Scara5* (D, red) or immunostained for CLEC3B (E, red).

(G and H) Uninjured nail bed dermis sections probed by FISH for *Nrg2* (G, red) or *Sfrp2* (H, red).

(J and K) Uninjured digit tip periosteum and bone immunostained for SP7 (J, green) or probed by FISH for *Dmp1* (K, red).

(L–O) scRNA-seq analysis of 10 and 14 DPA digit tips. (L and M) t-SNE visualizations of 11–14 cell clusters each at 10 (L) and 14 DPA (M) showing cell types identified by marker genes such as *Pdgfrb*, *Pdgfra*, or *Rgs5* (N and O).

(legend continued on next page)

with epithelial and Schwann cells at 10 and 14 DPA, respectively. For the two 14 DPA replicates, cells were intermingled within clusters, cell-type proportions were similar, and this was not altered with batch correction (Figures S2N and S2O). Compared with the uninjured, regenerating digit tips contained more immune cells (14%–37% versus 3%) and more proliferating cells (Figure 2P, 8%–12% versus 1% as predicted by Cyclone) consistent with previous morphological studies (Fernando et al., 2011; Johnston et al., 2016).

To compare uninjured and regenerating mesenchymal cells, we combined and analyzed transcriptomes from *Pdgfra*-positive clusters in all datasets (3,126 cells; 2,004 uninjured, 444 10 DPA, and 678 14 DPA). We identified 8 *Pdgfra*-positive clusters and one small *Pdgfra*-negative, *Sox10*-positive Schwann cell cluster that was not considered further (Figures 3A, 3B, S3A, and S3B). This analysis supported two conclusions. First, uninjured and regenerating mesenchymal cells were segregated, with 99.6% of uninjured cells in clusters 1, 3, 4, 6, and 7 and 97.4% of regenerating cells in clusters 2, 5, and 8. A similar segregation of uninjured and regenerating cells was observed following batch correction (Figure S3C). Further support for the conclusion that these two populations were distinct came from correlation analyses ( $r = 0.81$ – $0.93$  and  $\rho = 0.82$ – $0.93$ , uninjured versus regenerating clusters), statistical analysis of gene signature similarities or differences ( $p < 1 \times 10^{-10}$ ; see STAR Methods), and uniform manifold approximation and projection (UMAP)-based clustering and hierarchical clustering based upon average differential gene expression (Figures 3C and S3D). The only exceptions to this segregation were two mixed clusters, *Nrg2*-positive nail bed dermis cells (7) and a small osteochondrogenic cluster (8), expressing *Col2a1*, *Chad*, and *Bglap*. The second conclusion was that 10 and 14 DPA cells were similar but not identical to each other (Figures 3A and 3B). Specifically, 81% of cluster 5 cells were from 10 DPA, whereas 89% of cluster 2 cells were from the 14 DPA runs. Both 14 DPA replicates were clustered similarly (86% run 1 and 79% run 2 cells in cluster 2). Hierarchical clustering and correlation analyses as well as statistical analysis of gene signature similarities or differences further supported the conclusion that 10 DPA cluster 5 and 14 DPA cluster 2 were distinct (Figure 3C;  $r = 0.97$ ,  $\rho = 0.96$ ;  $p < 1 \times 10^{-10}$ ). Thus, regenerating cells progress transcriptionally over time.

### Identification of a Mesenchymal Blastema Transcriptional Signature

To define a transcriptional signature for blastema mesenchymal cells, we analyzed the uninjured, 10 and 14 DPA datasets for genes enriched in *Pdgfra*-positive clusters relative to all other clusters ( $p < 0.01$  family-wise error rate (FWER)). Of 2,871 identified genes, 1,541 were enriched only at 10 and/or 14 DPA and, after excluding proliferation-associated genes, 211 were expressed in  $\geq 10\%$  of regenerating but  $\leq 4\%$  of uninjured mesenchymal cells (Figure S3E; Tables S1 and S2); 197 of these were detected, on average, in 19.3-fold more regenerating versus uninjured cells, and 14 were detected only in regenerating cells.

Examples of these were *Arsi*, *Arxes1*, *Colq*, *Fbn2*, *Grem1*, *Lrrc17*, and *Npr3*, as best visualized by t-SNE overlays and violin plots (Figures 3D, 3E, and S3F). We also identified 19 genes expressed in 4%–10% of uninjured cells and  $\geq 10$ -fold more regenerating cells. These were expressed, on average, in 16.3-fold more regenerating than uninjured cells and included *Acan*, *Ltbp2*, and *Pdgfc* (Table S2).

We used this 230 gene signature to validate the 10 and 14 DPA cluster 2/5 cells (Figures 3A and 3B) as mesenchymal blastema cells, analyzing digit tip sections from mice expressing nuclear EGFP in *Pdgfra*-positive cells (*Pdgfra*<sup>EGFP/+</sup> mice) (Figures 3F, 3G, S3G, and S3H). Two signature gene proteins, ARSI and LTBP2, were broadly expressed in the 14 DPA blastema but not uninjured EGFP-positive cells. A similar pattern of expression was seen with FISH on wild-type sections for 5 signature mRNAs, *Arsi*, *Ltbp2*, *Grem1*, *Lrrc17*, and *Fbn2*, and a positive control, *Col11a1*, which is expressed in 95% of cluster 2/5 cells (Figures 3H–3M and S3I–S3N).

### Mesenchymal Cells Acquire the Blastema Transcriptional State Early during Blastema Formation and Lose It as Regeneration Finishes

We asked how the blastema transcriptional state changed over time. We first sequenced 1,197 cells at 7 DPA when a *Pdgfra*-positive blastema is initially observed (see Johnston et al., 2016). Analysis (Figure S3O) showed that 9 of 11 clusters included immune cells and osteoclasts (86.7% of total cells; clusters 1, 2, 3, 4, 6, 7, 8, 9, and 11), consistent with previous reports (Fernando et al., 2011). The remaining 2 clusters included *Pdgfra*-positive cells (5) (9.3% total cells) and vasculature-associated cells (10).

We combined and analyzed transcriptomes from the 7 DPA cluster 5 with all other *Pdgfra*-positive transcriptomes. This analysis (Figures 3N and 3O) and statistical analysis of gene signature similarities or differences ( $p = 0.55$ ) showed that 7 DPA cells were transcriptionally similar to 10 DPA cells. Of the 7 clusters in this dataset, two (2 and 4) included 99.6% of regenerating cells, and one of these (4) largely consisted of intermingled 7 and 10 DPA cells (84.3%). The other cluster (2) included predominantly 14 DPA cells (89.6%). The uninjured cells (98.9%) were instead in clusters 1, 3, 5, and 6, and there was one small osteochondrogenic cluster of mixed origin (7) (60 cells).

We further compared transcriptomes using pseudo-temporal ordering via Monocle. This defined a single major trajectory (Figures 3P and S3P). Intermingled 7, 10, and 14 DPA cells were at one end and 14 DPA cells extended and met the uninjured cells, which comprised the remainder of the trajectory with several branch points indicative of different adult digit mesenchymal cell types. Quantification confirmed segregation of the blastema and uninjured cells; 97%–99% of blastema cells, but only 3.2% of uninjured cells, were located prior to branch point 1 in trajectory state 7 (box in Figures 3P and S3P).

These analyses indicate that mesenchymal cells acquire a unique gene signature as soon as the blastema forms. To ask

(P) Cyclone analysis for predicted cell-cycle status of uninjured, 10 DPA and 14 DPA cells (yellow, G1; green, S; purple, G2/M). Numbers indicate % of cells in S and G2/M. For t-SNE gene expression overlays, cells are coded as per the adjacent color keys. All sections were counterstained for Hoechst 33258 (white nuclei). Low-magnification images of (D), (E), (G), (H), (J), and (K) are in Figures S2G, S2H, and S2J–S2M. Scale bars, 10  $\mu$ m. See also Figure S2.

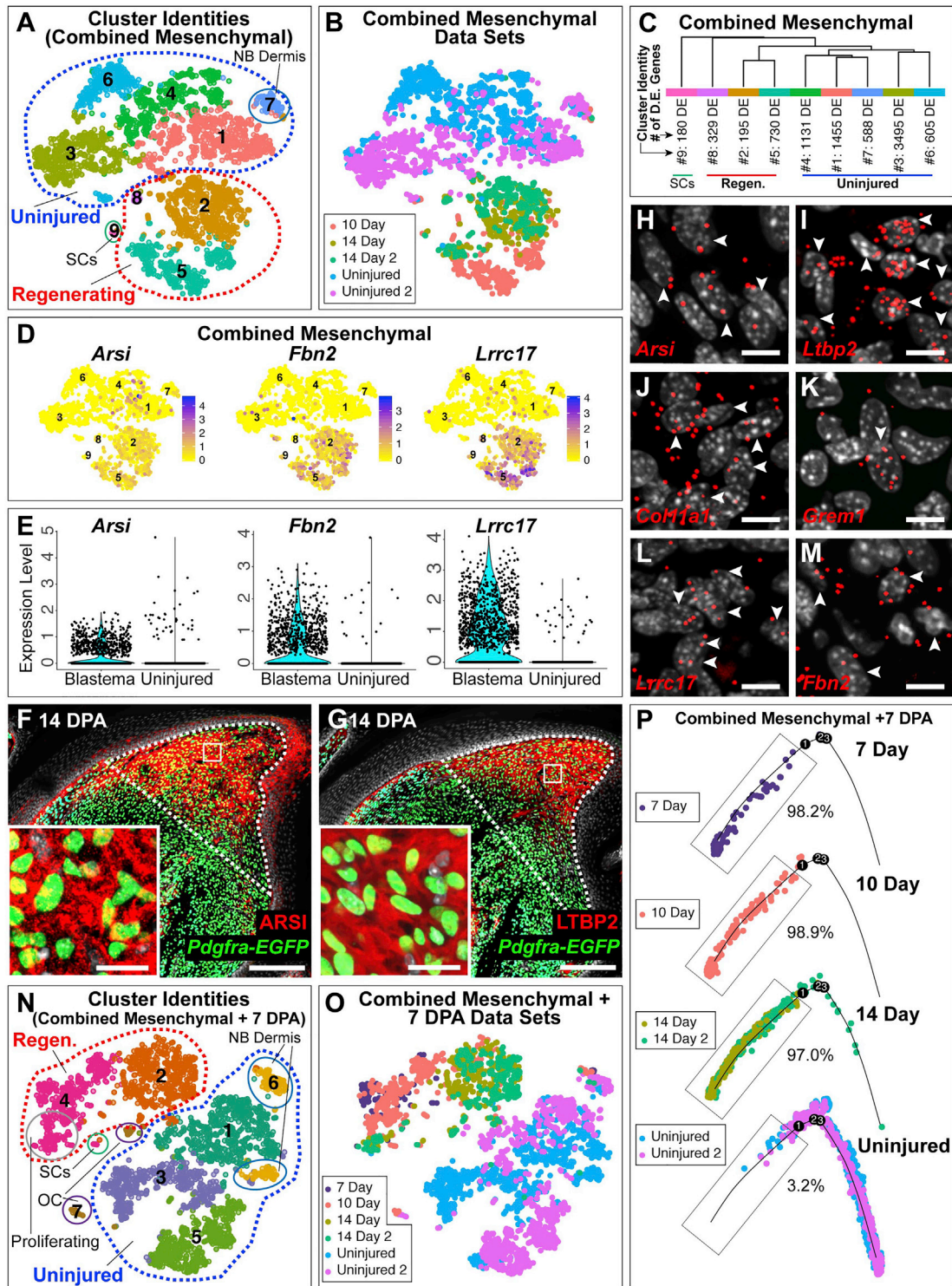


**Figure 3. Identification of a Mesenchymal Blastema Transcriptional Profile**

(A–E) Transcriptomes of cells in *Pdgfra*-positive clusters in Figure 2A (uninjured), 2L (10 DPA), and 2M (14 DPA), were extracted, combined, and reanalyzed. (A and B) t-SNE visualization of cell clusters. In (A), uninjured versus regenerating cells are outlined in blue versus red, and nail bed (NB) dermis and Schwann cells (SCs) are annotated. In (B), cells are color coded for dataset of origin. (C) Hierarchical clustering based upon the top 486 differentially upregulated genes per cluster ( $p < 0.01$ , FWER). Differentially expressed (DE) genes per cluster are also shown. (D and E) t-SNE visualizations (D) and violin plots (E) showing expression of *Arsi*, *Fbn2*, and *Lrrc17* in uninjured versus regenerating (blastema) cells. Cells in (D) are coded as per the adjacent color keys.

(legend continued on next page)

if they lose it as regeneration ensues, we sequenced 4,562 cells from 28 DPA when regrowth is finished but remodeling is ongoing and 4,602 cells from 56 DPA when regeneration is complete. In both datasets, we identified clusters containing *Pdgfra*-positive mesenchymal cells, endothelial cells, Schwann cells, epithelial cells, VSM/pericyte cells, and immune cells (Figures S4A and S4B). We extracted transcriptomes from *Pdgfra*-positive clusters and combined these with *Pdgfra*-positive transcriptomes from all other datasets. Trajectory analysis showed that the mesenchymal blastema transcriptional state was largely lost as regeneration finished (Figures 4A and S4C). Specifically, a portion of the trajectory (state 1, boxed region) containing 98% of blastema cells and 9.6% of uninjured cells included only 27% and 13% of the 28 and 56 DPA cells, respectively. The rest were intermingled with uninjured cells. Analysis of blastema signature genes further supported this conclusion (Figure 4B). At 28 DPA, 69 of 230 signature genes were expressed at uninjured levels, with the rest expressed, on average, at 19% of peak blastema levels. By 56 DPA, 137 signature genes were expressed at uninjured levels and 44 at  $\leq 10\%$  of peak blastema levels.

### Blastema Cells Express Mesenchymal Development Genes but Do Not Acquire an Embryonic Digit State

We asked if digit tip blastema cells are similar to embryonic digit mesenchymal cells, as has been reported for axolotl limb regeneration (Gerber et al., 2018). To do so, we sequenced and analyzed 3,908 embryonic day 11 (E11) hind limb cells, 3,293 E14 hind limb digit cells, and 2,700 P3 digit tip cells, the latter a time of tissue growth and differentiation. We identified *Pdgfra*-positive clusters in each dataset and combined and analyzed them together. As predicted (Karamboulas et al., 2010; Wyngaarden, and Hopyan, 2008), limb or digit mesenchymal precursors were largely transcriptionally distinct at E11, E14, and P3 and transitioned from proliferative expansion to generating bone, cartilage, and dermis over this time frame (Figures 4C–4F, S4D, and S4E). At E11, 40% of cells were proliferative and clusters were very similar to each other, expressing early limb genes such as *Pitx*, *Six4*, and *Tbx4* ( $r = 0.97$ – $0.99$  and  $\rho = 0.97$ – $0.98$  for all correlative comparisons). At E14, proliferating cells decreased to 19%, and chondrogenic genes such as *Acan* and *Foxa3* started to be expressed. By P3, only 7% of cells were proliferating, and clusters were more distinct (Figures 4E and 4F;  $r = 0.85$ – $0.95$  and  $\rho = 0.86$ – $0.93$ ). Cluster 7 expressed chondrogenic genes such as *Acan* and *Comp*; cluster 8 expressed osteogenic precursor genes such as *Wnt16*, *Sp7/Osterix*, *Alpl*, and *Scx*; and cluster 9 expressed developing dermal or CT genes such as *Twist2*, *Cd34*, and *Thy1*.

We used 3 approaches to compare developing cells to *Pdgfra*-positive blastema cells. First, we analyzed blastema signature

genes (Table S2). Only 126 of 230 (55%) genes were expressed in  $\geq 10\%$  of cells at one or more developmental time points. Second, we combined developing *Pdgfra*-positive cells with those from all other datasets and performed Monocle analysis. This correctly predicted the developmental time course (Figure 4G), starting with intermingled E11 and E14 cells followed by P3 cells and ending with uninjured adult cells (A–B–C). There was also a branch point in the P3 cells (A'–B). Notably, blastema cells did not intermingle with the embryonic cells on this trajectory (Figures 4H and S4F). Instead, they were mixed with P3 cells on the branched trajectory (A'–B) and extended to and mixed, to some degree, with the uninjured cells.

Third, we performed correlation analyses that consider all detected genes instead of just the most variable genes used by Monocle. Analysis of average gene expression showed that the blastema clusters were poorly correlated with E11 clusters ( $r = 0.76$ – $0.81$  and  $\rho = 0.73$ – $0.80$ ), somewhat better correlated with E14 clusters ( $r = 0.82$ – $0.86$  and  $\rho = 0.78$ – $0.85$ ), and were best correlated with, although still distinct from, P3 clusters ( $r = 0.90$ – $0.91$  and  $\rho = 0.86$ – $0.92$ ). We also performed single-cell correlational analysis. As comparators, we determined average gene expression for early (7 and 10 DPA) and peak (14 DPA) blastema cells, adult uninjured cells, and, based upon the trajectory analysis, P3 cells. We compared each single-cell transcriptome with the averaged datasets using Pearson's correlation and used the resultant  $r$  values to assign a two-dimensional coordinate to each cell. This analysis (Figure 4I) showed that blastema cells formed a continuous, overlapping trajectory on the x axis from 7 or 10 to 14 DPA. On the y axis, almost all blastema cells were more similar to P3 than to adult cells. Notably, the blastema cells did not overlap with the embryonic cells. However, a subset of 14 DPA blastema cells overlapped with one of two P3 cell groups.

To better understand the similarity between 14 DPA blastema and P3 mesenchymal cells, we combined them. t-SNE-based clustering with and without batch correction (Figures 4J and S4G) segregated the two populations, with 4 mutually exclusive clusters each of P3 versus 14 DPA cells that were similar to those seen in other analyses of the same datasets (see Figures 3N and 4C). Hierarchical and correlation analyses indicated that 14 DPA cluster 1 and P3 osteogenic precursor cluster 3 were the most similar of the blastema versus neonatal clusters (Figures 4K and S4H;  $r = 0.96$  and  $\rho = 0.94$ ) but that there were significant differences as confirmed by statistical analysis of gene signature similarities or differences ( $p < 1 \times 10^{-10}$ ). For example, P3 cluster 3 was specifically enriched for some osteogenic precursor genes such as *Wnt16*, *Sema3a*, and *Scx*, whereas 14 DPA cluster 1 was instead enriched for uninjured adult mesenchymal cell genes such as *Spon1*, *Crispld2*, and

(F and G) 14 DPA *Pdgfra*<sup>EGFP+</sup> sections, showing EGFP (green) and immunostaining for ARSI (F, red) and LTBP2 (G, red). Hatched lines outline non-epithelial regenerating tissue and insets show boxed regions.

(H–M) 14 DPA sections analyzed by FISH for *Arsi* (H), *Ltbp2* (I), *Col11a1* (J), *Grem1* (K), *Lrcc17* (L), and *Fbn2* (M). Arrowheads denote FISH-positive cells (red dots). Low-magnification images are in Figures S3I–S3N.

(N and O) t-SNE visualization of clusters from uninjured, 7 DPA, 10 DPA, and 14 DPA *Pdgfra*-positive cluster transcriptomes (Figure 3A plus cluster 5 in Figure S3O). In (N), uninjured versus regenerating cells are outlined in blue versus red, and in (O), cells are color coded for dataset of origin. OC, osteochondrogenic.

(P) Pseudo-time ordering of transcriptomes from (N) with time points shown separately (total combined dataset is shown in Figure S3P). Numbers indicate % of cells in the state 7 trajectory region (boxed). Sections were counterstained with Hoechst 33258 (white). Scale bars, 200  $\mu$ m in (F) and (G), 20  $\mu$ m (high-magnification insets), and 10  $\mu$ m in (H) and (M).

See also Figure S3.

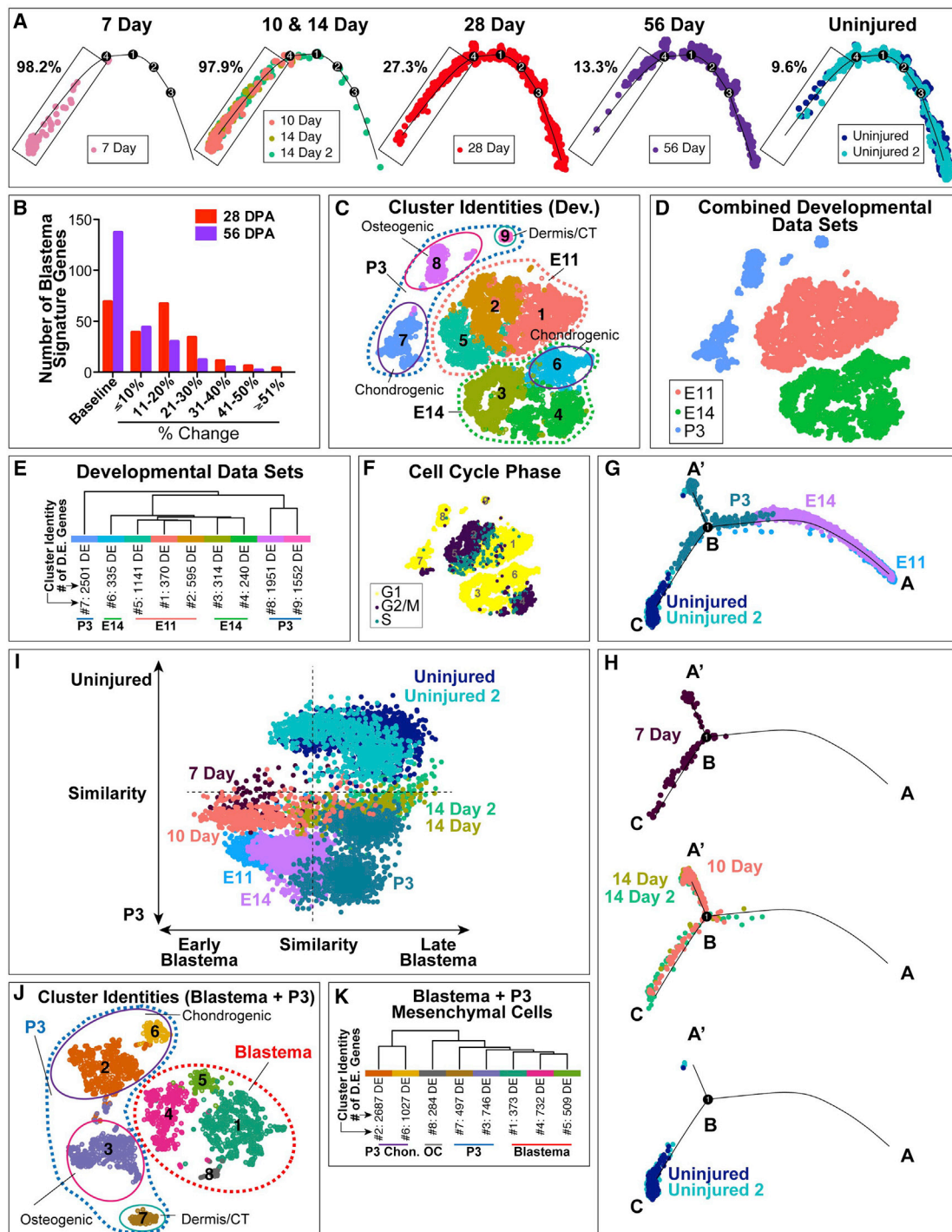


**Figure 4. The Blastema Is Transcriptionally Distinct from Developing Digit Tip Mesenchymal Cells**

(A) Pseudo-time ordering of 7, 10, 14, 28, and 56 DPA plus uninjured *Pdgfra*-positive cells, showing individual time points (combined is in Figure S4C). Numbers indicate % of cells in the state 1 trajectory region (boxed).

(B) Bar graph showing blastema signature genes expressed in 28 (red) and 56 (purple) DPA cells at levels similar to uninjured cells (baseline) or higher than uninjured but  $\leq 10\%$ , 11%–20%, 21%–30%, 31%–40%, or  $\geq 51\%$  of peak blastema levels.

(C–F) scRNA-seq was performed on E11 hind limbs, E14 digits, and P3 digit tips; datasets were analyzed via the pipeline; and *Pdgfra*-positive cluster transcriptomes were extracted, combined, and reanalyzed. (C and D) t-SNEs showing clusters (C) and datasets of origin (D). Chondrogenic, osteogenic and dermis or CT clusters (defined by marker genes) are annotated. (E) Hierarchical clustering based on the top 299 differentially upregulated genes ( $p < 0.01$ , FWER) per cluster. Differentially expressed (DE) genes per cluster are also shown. (F) Cyclone analysis to predict cell-cycle status, color coded as in the adjacent key.

(legend continued on next page)

*Ly6a* (Figures S4H and S4I). Thus, blastema cells express many mesenchymal developmental genes, but they do not recapitulate development.

### Mesenchymal Cells in the Non-regenerative Digit Tip Partially Acquire a Blastema Transcriptional State

The blastema transcriptional state likely includes genes associated with both tissue repair and regeneration. To distinguish between these responses, we performed non-regenerative amputations that remove the nail bed (Figure 5A). We confirmed that these did not result in regeneration and showed, using *Pdgfra*<sup>EGFP/+</sup> mice, that at 14 DPA there was an EGFP-positive CT cap on the bone stump (Figure 5B). We then isolated tissue distal to the non-regenerative amputation plane and sequenced and analyzed 5,352 14 DPA cells and 2,306 10 DPA cells from 2 different runs. This analysis (Figures 5C and 5D) identified clusters containing *Pdgfra*-positive mesenchymal cells, endothelial cells, VSM/pericytes, epithelial cells, and immune cells at both time points and Schwann cells at 14 DPA. Cells from the two 10 DPA replicates were intermingled in all clusters with similar proportions of cell types (Figure S5A), arguing against batch effects.

We compared regenerative and non-regenerative mesenchymal cells by combining and analyzing transcriptomes from *Pdgfra*-positive clusters in these datasets. This defined 6 *Pdgfra*-positive clusters and one small Schwann cell cluster (7) that was not considered further (Figures 5E and 5F). Two clusters contained only regenerative cells, one (3) with 95.3% 10 DPA cells and the other (1) with 88.9% 14 DPA cells. Two other clusters contained intermingled 10 and 14 DPA non-regenerative cells (2 and 4). These regenerative-only and non-regenerative-only clusters were also seen with UMAP-based clustering and were not altered by batch correction (Figures S5B and S5C). The remaining 2 clusters, one proliferative (5) and one osteochondrogenic (6), contained both regenerative and non-regenerative cells (Figures S5D and S5E). Hierarchical clustering (Figure S5F) and statistical analysis of gene signature similarities or differences ( $p < 1 \times 10^{-10}$ ) confirmed that the regenerative versus non-regenerative clusters were transcriptionally distinct from each other.

Two lines of evidence indicated that non-regenerative cells acquired some but not all aspects of a regenerative state. First, 102 of 230 blastema signature genes (44%) were expressed in non-regenerative cells at levels similar to or greater than the blastema cells ( $\geq 51\%$  on a trajectory from uninjured to blastema cell levels), as exemplified by *Prickle1* and *Ccdc8* (Figure 5G; Table S3). Second, trajectory analysis with the E11, E14, P3, and adult uninjured *Pdgfra*-positive cells showed that, by contrast to the regenerative cells, many non-regenerative cells had shifted away from the uninjured cells toward the P3 cells but

that very few had intermingled with the neonatal cells (Figures 5H, 5I, and S5G).

### Identification of Genes Enriched in Regenerative versus Non-regenerative Mesenchymal Cells

To define genes that distinguish regenerative versus non-regenerative cells and thus might be involved in regeneration, we identified mRNAs enriched in *Pdgfra*-positive clusters for the 10 and 14 DPA total cell datasets ( $p < 0.01$ , FWER). Of 2,353 identified mRNAs, 1,480 were enriched only in regenerative cells (Figure S5H; Table S4). Of these, we excluded proliferation genes and genes expressed in  $<7\%$  of regenerating cells. We then identified 123 regeneration-enriched mRNAs detected in  $\leq 10\%$  of non-regenerative cells and  $\geq 2$ -fold more regenerating cells (Table S5). Two of these were not detected in non-regenerative cells (*Ptprt* and *Zic5*), and the rest were detected, on average, in 6.3-fold more regenerative cells (Table S5). The regeneration genes were also enriched an average of 12.7-fold relative to uninjured cells and, consistent with this, 64 (52%) were also blastema signature genes.

We used the Biological Networks Gene Ontology (BiNGO) tool (Maere et al., 2005) to identify potential functions of the regeneration-enriched genes (version 3.0.3) (Maere et al., 2005). Top terms were all associated with development and differentiation, and the top 12 included multicellular organismal development, anatomical structure morphogenesis, developmental process, tissue development, and embryonic morphogenesis ( $p$  values ranging from 11 to  $22.6 \times 10^{-10}$ ) (Figure S5I; Table S6). Consistent with this, 65 of 123 regeneration-enriched genes were expressed in  $\geq 10\%$  of the E11, E14, and/or P3 limb or digit mesenchymal cells (Table S5). These included many known developmentally important genes such as the transcription factors *Dlx5*, *Lhx9*, and *Msx2* and the ligand *Bmp5* (Figures 5J and S5J; Table S5) as well as genes involved in digit tip regeneration such as *Lgr6*, ligands of the *Bmp*, *FGF* and *Wnt* families, and *Msx* transcription factors (Lehoczky and Tabin, 2015; Yu et al., 2010, 2019; Takeo et al., 2013; Reginelli et al., 1995; Han et al., 2003). We validated this regeneration-enriched gene set by performing FISH for *Dlx5*, *Lhx9*, *Msx2*, and *Bmp5*. All 4 were expressed in many 10 and 14 DPA regenerative blastema cells but in few 10 and 14 DPA non-regenerative cap cells (Figures 5K, S5K, and S5L).

### Dermal Fibroblasts Contribute to the Blastema and to Bone Regeneration When Transplanted following Regenerative but Not Non-regenerative Amputations

To test the idea that the regenerative environment causes digit tip mesenchymal cells to acquire a blastema identity, we cultured dermal fibroblasts from neonatal *Pdgfra-CreERT*; *R26-LSL-TdT* mice, induced *Pdgfra-TdT*, and expanded cells

(G and H) Pseudo-time ordering of *Pdgfra*-positive cells from E11, E14, P3, 7 DPA, 10 DPA, 14 DPA, and uninjured datasets. Shown are the combined developmental datasets with adult uninjured datasets (G) and individual adult datasets (H) (total combined is in Figure S4F).

(I) Scatterplot showing correlation of single-cell transcriptomes (colors represent datasets) with P3 versus mature uninjured transcriptomes on the y axis and early (7 and 10 DPA) versus late (14 DPA) blastema on the x axis.

(J) t-SNE clusters of combined P3, 7 DPA, 10 DPA, and 14 DPA *Pdgfra*-positive cells. Regenerating (blastema) versus P3 cells are outlined by red versus blue. P3 clusters are annotated as in (C).

(K) Hierarchical clustering of the dataset in (J) based on the top 23 differentially upregulated genes ( $p < 0.01$ , FWER) per cluster. Differentially expressed (DE) genes per cluster are also shown.

See also Figure S4.

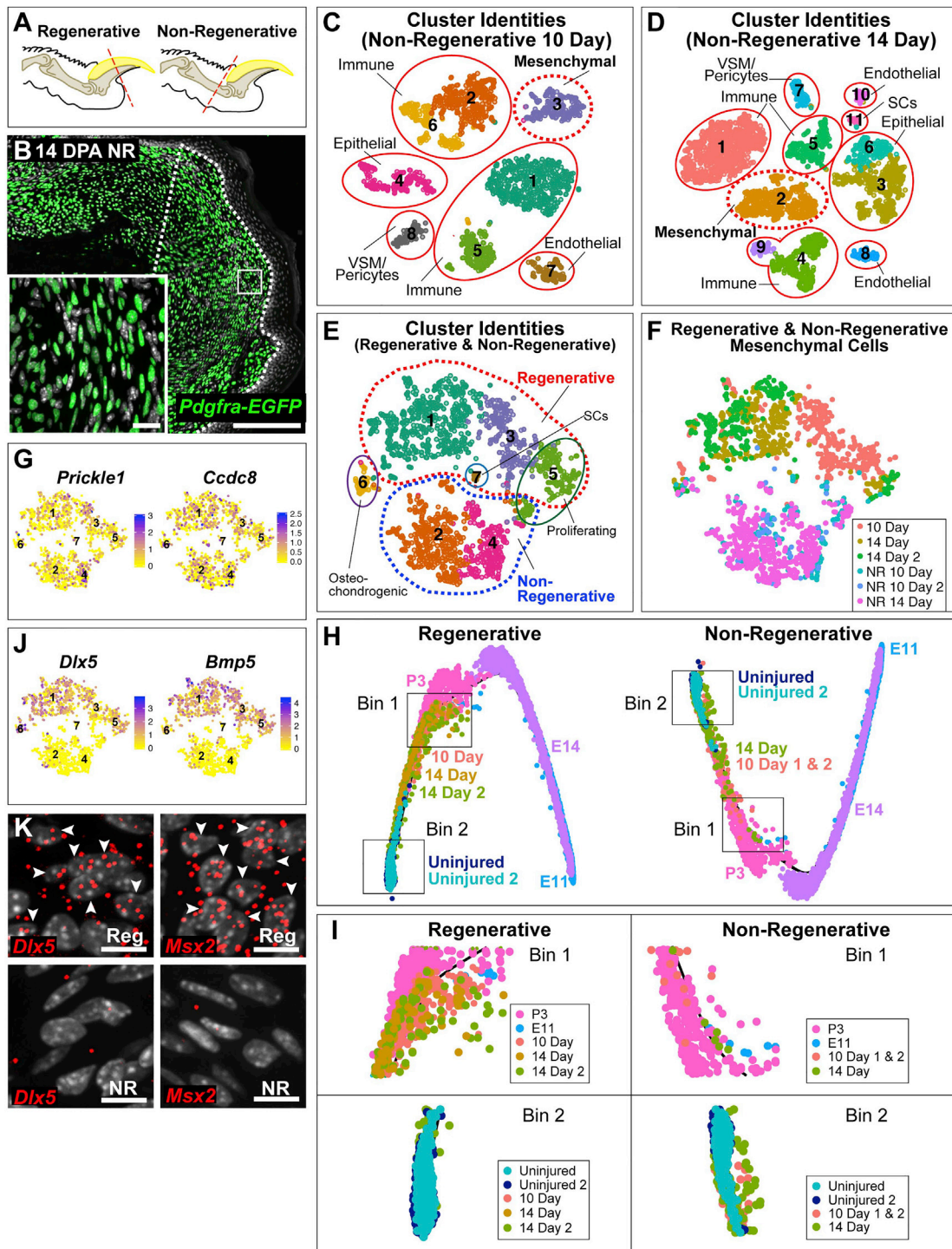


**Figure 5. Analysis of Non-regenerative Digit Tip Mesenchymal Cells**

(A) Schematic showing the non-regenerative versus regenerative amputation planes (red lines).  
 (B) Stitched image of a non-regenerative 14 DPA *Pdgfra*<sup>EGFP/+</sup> section showing EGFP (green) and Hoechst 33258-positive nuclei (white). White line outlines the non-epithelial CT cap, and inset shows the boxed region.  
 (C and D) t-SNE visualization of 10 DPA (C) and 14 DPA (D) non-regenerative clusters, annotated for cell types.  
 (E–G) *Pdgfra*-positive cluster transcriptomes from (C) and (D) and from 10 and 14 DPA regenerative datasets (Figures 2L and 2M) were combined and analyzed.  
 (E) Cluster t-SNE with regenerative and non-regenerative cells outlined in red versus blue. Osteochondrogenic, Schwann cell (SC), and proliferative clusters (defined by marker genes) are annotated.  
 (F) t-SNE showing the datasets of origin. (G) t-SNE expression overlays for *Prickle1* and *Ccdc8*, coded as per the adjacent color keys.

(legend continued on next page)

adherently. These cells were positive for TdT but not for the blastema proteins ARSI, LTBP2, or ALPL (Figure S6A). We then transplanted the cells 6 days after regenerative or non-regenerative amputations (Figure 6A). In regenerating 14 DPA digit tips, the blastema contained TdT-positive cells that expressed ARSI, LTBP2, and ALPL and the regeneration-enriched mRNAs *Bmp5*, *Msx2*, *Dlx5*, and *Lhx9* (Figures 6B–6D and S6B), supporting the idea that these transplanted fibroblasts acquired at least some aspects of the blastema state. By 28 DPA, the osteocalcin-positive regenerated bone contained DMP1-positive, TdT-positive osteocytes within bone lacunae (Figures 6E, 6F, S6C, and S6D). TdT-positive cells were also present in the dermis, where they expressed the dermal or CT markers THY1 and VERSICAN (VCAN) but not DMP1 or CD31 (Figures 6G, S6E, and S6F). By contrast, after non-regenerative amputations at 14 DPA, TdT-positive cells were present in the CT cap, but they expressed little or no *Msx2*, *Bmp5*, *Dlx5*, or *Lhx9* mRNA (Figures 6H and S6G). By 28 DPA, TdT-positive cells were seen in the CT between the bone stump and epidermis, where they appropriately expressed CD34 and THY1 (Figures 6I, 6J, S6H, and S6I).

### Bone-Lineage Cells Divide and Acquire a Blastema Transcriptional Phenotype following Digit Tip Amputation

To ask if endogenous lineage-biased mesenchymal cells contribute to regeneration as did transplanted fibroblasts, we used *R26-LSL-TdT* mice that carried *CreERT2* driven by *Dmp1* promoter or enhancer regions. This transgene is expressed specifically in osteocytes and bone-lining cells thought to be osteoblasts (Kim et al., 2012; Torreggiani et al., 2013). Consistent with this, 4 days post-tamoxifen (Figure 6K), uninjured adult digit tip osteocytes were TdT positive (91% ± 0.6%; n = 3) as were bone-lining cells and a few SP7-positive progenitors associated with bone vasculature (5% of total TdT-positive cells) (Sivaraj and Adams, 2016).

To better define these TdT-positive cells, we sequenced and analyzed 1,525 cells 10 days post-tamoxifen. As in other uninjured datasets (Figure 2A), we identified endothelial cells, VSM/pericyte cells, epithelial cells, Schwann cells, immune cells, and 3 clusters of *Pdgfra*-positive cells (330/991 total cells) (Figure S6J). One mesenchymal cluster (2) included dermal or CT cells expressing *Clec3b* and *Scara5* and another (5) *Nrg2*-positive nail bed dermis cells. The third cluster (6) included bone-lineage cells enriched for *Dmp1*, *Bglap*, *Bglap2*, *Sp7*, and *Spp1* (8% of total cells). This bone cluster included almost all *tdT*-positive cells (Figure 6L) except for 2 and 3 cells in the dermis or CT and VSM/pericyte clusters, respectively. Consistent with this, correlation analysis (Figure 6M;  $r = 0.94$  and  $\rho = 0.89$ ) showed that *tdT*-positive cells were enriched for osteoblast genes relative to *tdT*-negative mesenchymal cells. On a single-cell level,

90%–100% of *tdT*-positive cells expressed *Bglap*, *Bglap2*, *Pth1r*, *Mef2c*, and *Sox4*; 50%–60% expressed *Ibsp*, *Spp1*, and *Sp7*; and all but one co-expressed at least 5 of these mRNAs.

These data indicate that the *tdT*-positive, *Pdgfra*-positive cells are osteoblasts/osteocytes. We asked what happened to these tagged cells during regeneration. We amputated digit tips 10 days post-tamoxifen and injected EdU in some mice at 13 DPA. At 14 DPA, TdT-positive cells were found in the blastema and uninjured bone compartment (Figure 6N) and comprised 26% of total non-epithelial regenerating cells. TdT-positive cells within the blastema, but not the uninjured digit tip, were positive for ARSI and LTBP2 and for the blastema/regeneration mRNAs *Grem1*, *Col11a1*, *Bmp5*, *Msx2*, and *Dlx5* (Figures 6O and 6P). 19% of regenerative TdT-positive cells were also EdU positive (Figure 6Q), in contrast to the uninjured digit tip with only 1–2 double-positive cells per section.

To definitively establish that *Dmp1CreERT2*-TdT-positive cells acquired a blastema state, we sequenced and analyzed 5,149 14 DPA cells from mice treated with tamoxifen before injury. We identified clusters containing *Pdgfra*-positive mesenchymal cells, endothelial cells, VSM/pericyte cells, Schwann cells, and immune cells (Figure S7A). Analysis of *Pdgfra*-positive cluster transcriptomes (Figure 7A) identified 6 mesenchymal clusters that expressed all the blastema signature and regeneration-enriched genes (Figure 7B; Table S7). One other cluster (7) was positive for both immune and mesenchymal genes and was not considered further. Hierarchical and correlation analyses showed that the regenerating clusters were all relatively similar ( $r = 0.94$ – $0.99$  and  $\rho = 0.93$ – $0.97$ ), except for cluster 3, which expressed mature osteochondrogenic genes such as *Chad*, *Col2a1*, *Bglap*, and *Dmp1* (Figures S7B and S7C).

20% of cells in this mesenchymal dataset were *Dmp1CreERT2-tdT* positive (Figure 7C). These were in all clusters but enriched in osteochondrogenic cluster 3 (33% *tdT* positive versus 16% total cells), likely reflecting TdT-positive cells in the bone compartment at 14 DPA (Figure 6N). *tdT*-positive cells were highly correlated with *tdT*-negative blastema cells (Figure 7D;  $r = 0.99$  and  $\rho = 0.98$ ). The 14 DPA *tdT*-positive cells were also very different from their uninjured *tdT*-positive osteoblast/osteocyte parental cells ( $r = 0.85$  and  $\rho = 0.82$ ) (Figure 7E), suggesting that they turned off bone-lineage genes as they acquired the blastema transcriptional state. Consistent with this, on a single-cell level, known bone-lineage genes such as *Lgr6*, *Col2a1*, *Dmp1*, and *Bglap* were depleted in *tdT*-positive and -negative cells outside of osteochondrogenic cluster 3 (Figures 7F, 7G, S7C, and S7D). By contrast, *tdT*-positive cells outside of cluster 3 expressed all blastema signature and regeneration-enriched genes at levels similar to *tdT*-negative blastema cells as exemplified by *Adamts9*, *Angpt1*, *Eva1a*, *Msx2*, and *Tnfrsf19* (Figure 7H; Table S7).

(H and I) Pseudo-time ordering of E11, E14, P3, and uninjured adult *Pdgfra*-positive cells combined with 10 and 14 DPA regenerative (left) or non-regenerative (right) datasets (injured versus developmental trajectories are in Figure S5G). (I) shows the bins in (H), which correspond to equivalent trajectory regions, at higher resolution.

(J) t-SNE overlays of cells in (E) for *Dlx5* and *Bmp5*, coded as per the adjacent color keys.

(K) 10 DPA regenerative (Reg) or non-regenerative (NR) sections analyzed by FISH for *Dlx5* and *Msx2* and stained for Hoechst 33258 (white nuclei). Arrowheads indicate FISH-positive cells (red dots). Low magnification images are in Figure S5L.

Scale bars represent 200  $\mu\text{m}$  in (B); 20  $\mu\text{m}$  (insets); and 10  $\mu\text{m}$  in (K).

See also Figure S5.

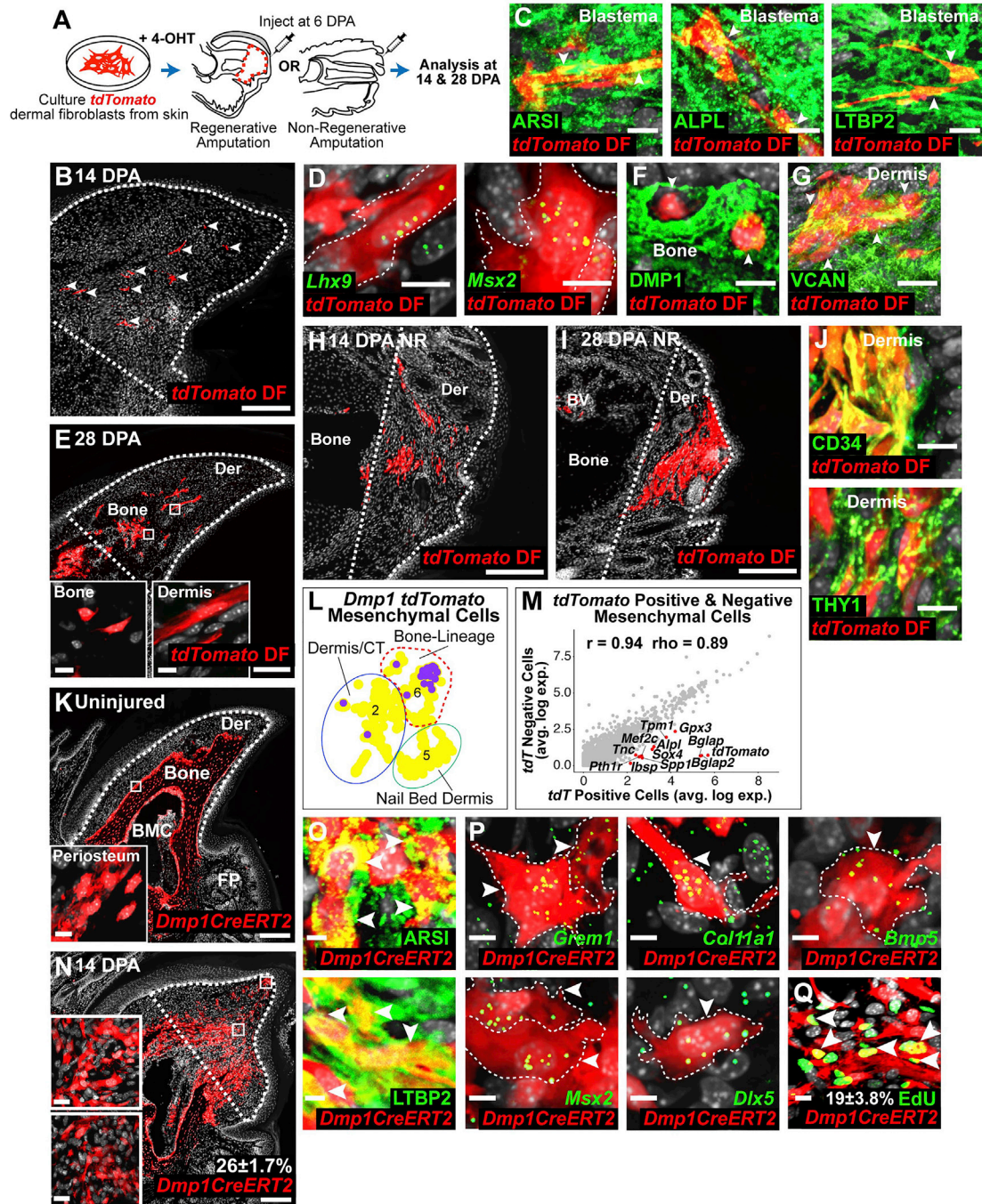


**Figure 6. Transplanted Fibroblasts and Endogenous Osteoblasts/Osteocytes Contribute to the Blastema**

(A) Schematic of transplantation experiments.

(B–D) Transplanted 14 DPA blastema sections showing TdTomato-positive cells (red, arrowheads in (B)) immunostained for ARSI, LTBP2, or ALPL (C, green) or analyzed by FISH for *Lhx9* or *Msx2* (D, green dots). Arrowheads (C) and hatched lines (D) indicate double-positive cells.

(E–G) Transplanted 28 DPA sections showing TdTomato (red) and DMP1 (green, F) or VCAN (green, G) immunostaining. Arrowheads indicate TdTomato-positive bone (F) and dermis (G) cells. Insets in (E) show boxed regions.

(H–J) Transplanted 14 (H) and 28 DPA (I and J) non-regenerative digits, showing TdTomato (red) and CD34 or THY1 immunostaining (J, green).

(K) Uninjured *Dmp1CreERT2*; *R26-LSL-TdTomato* digit tip, 10 days post-tamoxifen, showing TdTomato (red). Inset shows the boxed region.

(L) t-SNE expression overlay for TdTomato in uninjured digit tip *Pdgfra*-positive clusters defined by scRNA-seq analysis (shown in Figure S6J). TdTomato-positive and TdTomato-negative cells are purple and yellow, respectively.

(M) Pearson correlation analysis of average gene expression in TdTomato-positive (x axis) versus negative (y axis) cells from (L). Red denotes selected bone-lineage genes. Spearman correlation value is also indicated ( $\rho$ ).

(legend continued on next page)

### Osteoblasts/Osteocytes Contribute to Regeneration of Multiple Mesenchymal Tissues

To ask if *Dmp1CreERT2*-TdT-positive blastema cells contribute to tissue regeneration, we performed similar experiments and analyzed digit tips at 28 and 56 DPA. At both time points, proximal to the amputation plane TdT-positive cells were limited to the DMP1-positive bone compartment. However, within the regenerated tissue they were more broadly distributed and present both in bone lacunae and the dermis beneath the nail and K14-positive epidermis (Figures 7I–7K and S7E–S7G). These TdT-positive dermal cells were negative for DMP1, p75NTR, and CD31 but positive for PDGFR $\alpha$ , THY1, and VCAN (Figures 7J–7O and S7F–S7K). Thus, following amputation, *Pdgfra*-positive osteoblasts/osteocytes transition through a mesenchymal blastema state and contribute to the regeneration of bone and dermis.

### DISCUSSION

Here, we provide evidence that during adult digit tip regeneration, tissue-derived mesenchymal cells acquire a unique blastema state and then regenerate mesenchymal tissues without regard to their tissue of origin. Specifically, our findings support four key conclusions. First, we find that *Pdgfra*-expressing mesenchymal blastema cells derive from several different parental tissues. The *Dmp1*-based lineage tracing shown here indicates that 26% originate from osteoblasts/osteocytes, and we recently showed another 21% derive from mesenchymal cells within injured local nerves (Carr et al., 2019). We posit that the remaining half derive from the dermis or CT cells identified in the single-cell RNA sequencing (scRNA-seq) analyses because (1) transplanted dermal cells contribute to the blastema and regenerated tissues as shown here and (2) in amphibians, dermal fibroblasts contribute disproportionately to the blastema (Dunis and Namenwirth, 1977; Muneoka et al., 1986; Kragl et al., 2009; Currie et al., 2016). In this regard, digit tip regeneration requires an intact nail bed (Simkin et al., 2013; Takeo et al., 2013; Neufeld, and Zhao, 1995), and our data show that nail bed dermal cells are a unique population transcriptionally. We therefore speculate that because they continuously induce nail formation, the nail bed dermis cells are in a “primed” state that enables them to contribute robustly to and perhaps initiate the mesenchymal blastema.

A second key finding involves the transcriptional state of the digit tip blastema. During axolotl limb regeneration, blastema cells display an embryonic limb state (Gerber et al., 2018). By contrast, we show here that mammalian blastema cells do not recapitulate development, but instead acquire a unique regenerative transcriptional state as soon as the blastema forms and then lose it when regeneration is finished. At the same time,

mesenchymal cells lose their previous lineage bias, as exemplified by the *Dmp1-tdT* osteoblasts/osteocytes that we analyzed. What does the blastema transcriptional state “look” like? Our studies indicate that it includes many genes important for developing mesenchymal precursors as well as genes associated with adult mesenchymal tissue repair. We posit that this mix of developmental and adult repair transcriptional programs is what distinguishes mammalian blastema cells from their developing counterparts and potentially from blastema cells in highly regenerative organisms such as axolotls.

A third key finding is that non-regenerative digit tip mesenchymal cells acquire some but not all facets of a blastema transcriptional state. One explanation is that the shared genes reflect a repair response that occurs following any amputation, regenerative or not. A second explanation is that a regenerative response is initiated after any amputation, but it is then aborted in the absence of regeneration-specific cues. This latter explanation raises the exciting possibility that if we can identify the missing cues then perhaps we can exogenously promote regeneration. Our transplant studies support this idea; dermal fibroblasts contributed to fibrotic repair versus tissue regeneration when transplanted into non-regenerative versus regenerative environments. What then are the relevant environmental signals? One potential source is the wound epithelium, which forms immediately before blastema formation and communicates with the underlying mesenchyme via Wnt and FGF signaling (Takeo et al., 2013). Second is the nail bed dermis, which normally serves as an inductive signaling center (Takeo et al., 2013). Finally, Schwann-lineage cells from the injured nerve secrete growth factors such as PDGF-AA and Oncostatin M that directly promote blastema mesenchymal cell expansion (Johnston et al., 2016). Thus, a combination of spatially regulated signals from multiple cell types likely promotes initiation and expansion of the mesenchymal blastema.

Finally, we asked whether digit tip mesenchymal cells maintain their lineage bias during regeneration as is seen during muscle regeneration (Collins et al., 2005; Conboy et al., 2003) and for the digit tip *Myh11*-expressing vasculature-associated mesenchymal cells we studied here. Our data indicate this is not the case for regenerating mesenchymal cells. We show that endogenous bone-derived osteoblasts/osteocytes and transplanted dermal cells each contribute to the blastema and ultimately regenerate both bone and dermis. Thus, transiting through a blastema state somehow confers mesenchymal lineage flexibility, allowing cells to contribute to the regeneration of tissues other than their tissue of origin. Thus, if we can understand the environmental signals that promote acquisition of a mesenchymal blastema state, then this might tell us why regeneration fails in most mammalian situations and provide insights into therapeutic strategies for reversing this failure.

(N–Q) 14 DPA *Dmp1CreERT2;R26-LSL-TdT* sections from mice treated with tamoxifen before amputation, showing TdT (red) and ARSI and LTBP2 immunostaining (O, green) or FISH for *Grem1*, *Col11a1*, *Bmp5*, *Msx2*, and *Dlx5* (P, green dots). In (Q), the mouse was injected with EdU at 13 DPA and analyzed 24 h later for TdT (red) and EdU (green). Insets in (N) show boxed regions. Numbers in (Q) indicate % of TdT-positive cells also positive for EdU. Arrowheads and hatched lines denote double-labeled cells.

All images include Hoechst 33258 staining (white). Stitched images are shown in (B), (E), (H), (I), (K), and (N), and white outlines indicate the non-epithelial regenerating tissue or CT cap. BMC, bone marrow cavity; BV, blood vessel; Der, dermis; and FP, footpad. Scale bars, 200  $\mu$ m in (B), (E), (H), (I), (K), and (N); 20  $\mu$ m in (G) and insets in (N); 10  $\mu$ m in (C), (D), (F), (J), (Q), and insets in (E) and (K); and 5  $\mu$ m in (O) and (P).

See also Figure S6.

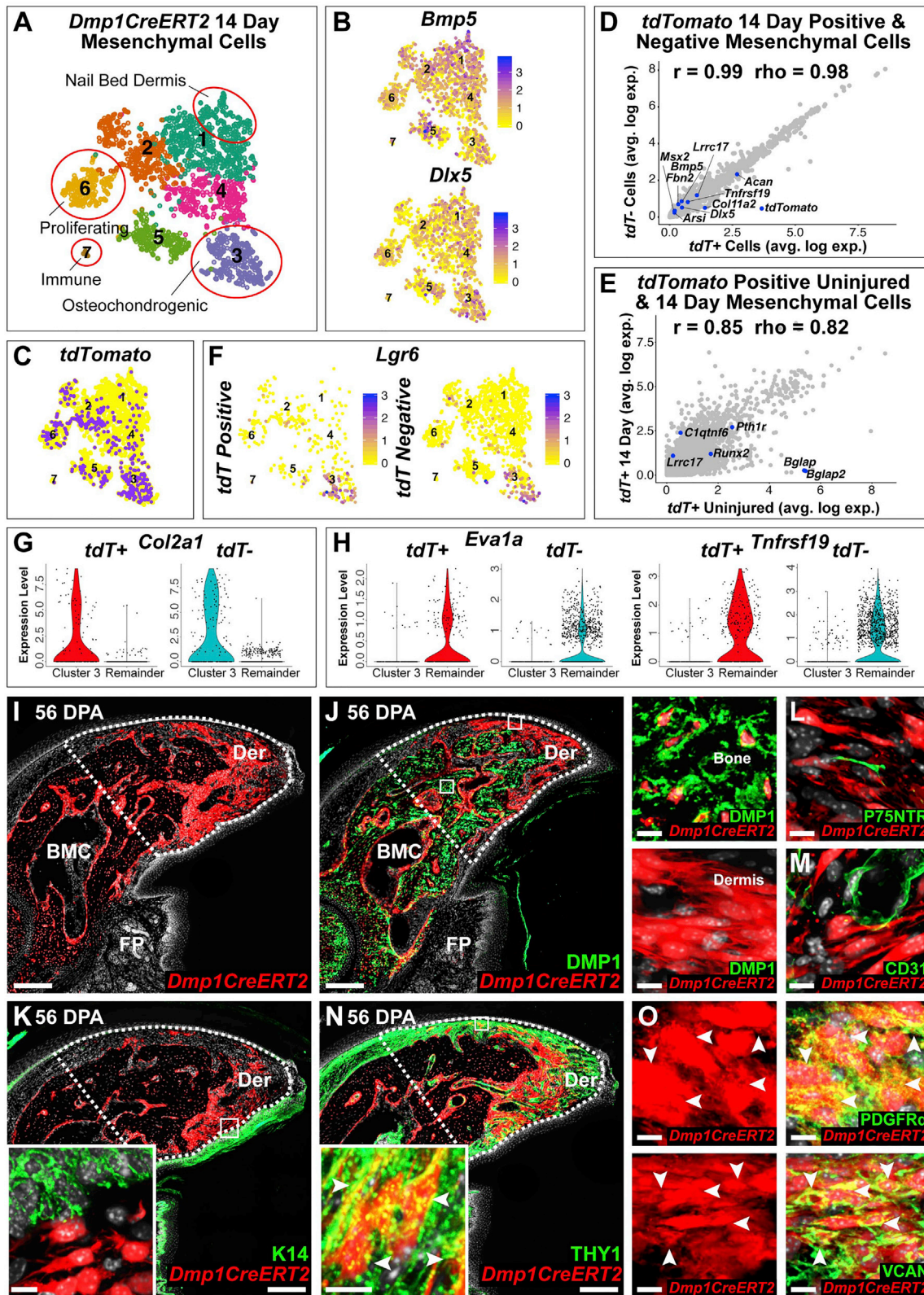


**Figure 7. Bone-Associated Cells Acquire a Blastema Transcriptional State and Contribute to Regeneration of Multiple Mesenchymal Tissues** (A–H) 14 DPA *Dmp1CreERT2*;R26-LSL-*TdTomato* distal digit tip cells from mice pre-treated with tamoxifen were sequenced and analyzed, and *Pdgfra*-positive cluster transcriptomes were extracted and reanalyzed. (A) t-SNE clusters, annotated. Immune denotes a cluster positive for *Pdgfra* and immune genes. (B and C) t-SNE

(legend continued on next page)

## STAR★METHODS

Detailed methods are provided in the online version of this paper and include the following:

- **KEY RESOURCES TABLE**
- **LEAD CONTACT AND MATERIALS AVAILABILITY**
- **EXPERIMENTAL MODEL AND SUBJECT DETAILS**
  - Mice
  - Dermal Fibroblast Cell Cultures
- **METHOD DETAILS**
  - Animal Surgeries & Tamoxifen Injections
  - EdU Labelling & Analysis
  - Dermal Fibroblast Transplant Studies
  - Tissue Preparation, Immunostaining & Microscopy
  - Antibodies
  - Fluorescence *In Situ* Hybridization (FISH)
  - Single-Cell Isolation & 10X Genomics
  - scRNA-seq Data Analysis
  - Identification of Transcriptional Signatures
  - Gene Ontology Analysis
- **QUANTIFICATION AND STATISTICAL ANALYSIS**
  - Morphometric Analyses of Bones & Nails
  - Quantification of Reporter-Positive Cells
  - Quantification of PDGFR $\alpha$ + Cells & Section Area
  - Quantification of *Dmp1CreERT2*-TdT+ Bone Lacunae
  - Quantification of *Dmp1CreERT2*-TdT+ Cells in Vessels
  - Statistical Testing of Populations in scRNA-Seq Data
  - Quantification of Monocle Trajectories
  - Quantification of Blastema Genes during Regeneration
  - Statistical Analysis
- **DATA AND CODE AVAILABILITY**

## SUPPLEMENTAL INFORMATION

Supplemental Information can be found online at <https://doi.org/10.1016/j.devcel.2019.12.004>.

## ACKNOWLEDGMENTS

This work was funded by CIHR and the CFREF “Medicine by Design” to F.D.M. and D.R.K. M.A.S. was funded by OIRM, CIHR, and HSC Restrcomp fellowships; S.A.Y. by a Lap-Chee Tsui Restrcomp fellowship; and M.J.B. by CIHR and NSERC studentships. We thank Rebecca Parsons, Dennis Aquino, and Neil Winegarden for technical assistance. We also thank Michael Underhill and Wilder Scott for sharing *tdTomato* sequences for alignment and Gary Bader for his computational advice.

## AUTHOR CONTRIBUTIONS

M.A.S. and N.M. conceptualized, performed, and analyzed the experiments and co-wrote the paper. M.A.S. performed the transplants, scRNA-seq experiments, and computational analysis and some of the lineage tracing. N.M. performed the lineage-tracing experiments and genetic ablation studies and assisted with the transplants. M.A.S. and N.M. performed the immunostaining and FISH. K.K. performed computational analysis and co-wrote the paper. M.J.B., S.A.Y., and A.G. performed and assisted with the computational analyses. A.A., in the lab of M.V.S., provided the hydrogel for transplants. F.D.M. analyzed the data and together with D.R.K. conceptualized the experiments and co-wrote the paper.

## DECLARATION OF INTERESTS

The authors declare no competing interests.

Received: June 17, 2019

Revised: November 11, 2019

Accepted: December 9, 2019

Published: January 2, 2020

## REFERENCES

- Benjamini, Y., and Hochberg, Y. (1995). Controlling the false discovery rate: a practical and powerful approach to multiple testing. *J. R. Stat. Soc. B* 57, 289–300.
- Borgens, R.B. (1982). Mice regrow the tips of their foretoes. *Science* 217, 747–750.
- Brockes, J.P., and Gates, P.B. (2014). Mechanisms underlying vertebrate limb regeneration: lessons from the salamander. *Biochem. Soc. Trans.* 42, 625–630.
- Brockes, J.P., and Kumar, A. (2002). Plasticity and reprogramming of differentiated cells in amphibian regeneration. *Nat. Rev. Mol. Cell Biol.* 3, 566–574.
- Carr, M.J., Toma, J.S., Johnston, A.P.W., Steadman, P.E., Yuzwa, S.A., Mahmud, N., Frankland, P.W., Kaplan, D.R., and Miller, F.D. (2019). Mesenchymal precursor cells in adult nerves contribute to mammalian tissue repair and regeneration. *Cell Stem Cell* 24, 240–256.e9.
- Collins, C.A., Olsen, I., Zammit, P.S., Heslop, L., Petrie, A., Partridge, T.A., and Morgan, J.E. (2005). Stem cell function, self-renewal, and behavioral heterogeneity of cells from the adult muscle satellite cell niche. *Cell* 122, 289–301.
- Conboy, I.M., Conboy, M.J., Smythe, G.M., and Rando, T.A. (2003). Notch-mediated restoration of regenerative potential to aged muscle. *Science* 302, 1575–1577.
- Currie, J.D., Kawaguchi, A., Traspas, R.M., Schuez, M., Chara, O., and Tanaka, E.M. (2016). Live imaging of axolotl digit regeneration reveals spatio-temporal choreography of diverse connective tissue progenitor pools. *Dev. Cell* 39, 411–423.
- Douglas, B.S. (1972). Conservative management of guillotine amputation of the finger in children. *Aust. Paediatr. J.* 8, 86–89.
- Dunis, D.A., and Namenwirth, M. (1977). The role of grafted skin in the regeneration of x-irradiated axolotl limbs. *Dev. Biol.* 56, 97–109.

overlays for *Bmp5*, *Dlx5* (both, B), and *tdT* (C). In (B), cells are coded as per the color keys, whereas in (C), *tdT*-positive and *tdT*-negative cells are purple and yellow, respectively. (D and E) Pearson correlation analysis of average gene expression in 14 DPA *tdT*-positive versus *tdT*-negative cells (D) or in 14 DPA versus uninjured *tdT*-positive cells (E). Blue denotes selected blastema signature, regeneration-enriched, or bone lineage genes. Spearman correlation values are also indicated (rho). (F) t-SNE overlay for *Lgr6* in *tdT*-positive (left) or *tdT*-negative (right) cells from the dataset in (A). Cells are coded as per the color keys. (G and H) Violin plots showing expression of *Col2a1* (G) or *Eva1a* and *Tnfrsf19* (H) in *tdT*-positive and *tdT*-negative cells in osteochondrogenic cluster 3 versus clusters 1, 2, 4, 5, and 6 (Remainder) in (A). Black dots represent individual cells. (I–O) 56 DPA *Dmp1CreERT2;R26-LSL-TdT* sections from mice treated with tamoxifen before amputation, showing TdT (red) and DMP1 (J), K14 (K), p75NTR (L), CD31 (M), THY1 (N), PDGFR $\alpha$  (O), or VCAN (O) immunostaining (green). Adjacent panels (J) and insets (K and N) show boxed regions. Stitched images are shown in (I), (J), (K), and (N), and white lines delineate the non-epithelial regenerated tissue. Arrowheads indicate double-labeled cells. All images show Hoechst 33258 staining (white). BMC, bone marrow cavity; Der, dermis; and FP, footprint. Scale bars, 200  $\mu$ m in (I), (J), (K), and (N); 20  $\mu$ m (insets); and 10  $\mu$ m in (L), (M), (O), and (J). See also [Figure S7](#).

- Fernando, W.A., Leininger, E., Simkin, J., Li, N., Malcom, C.A., Sathyamoorthi, S., Han, M., and Muneoka, K. (2011). Wound healing and blastema formation in regenerating digit tips of adult mice. *Dev. Biol.* *350*, 301–310.
- Gerber, T., Murawala, P., Knapp, D., Masselink, W., Schuez, M., Hermann, S., Gac-Santel, M., Nowoshilow, S., Kageyama, J., Khattak, S., et al. (2018). Single-cell analysis uncovers convergence of cell identities during axolotl limb regeneration. *Science* *362*, eaaq0681.
- Hamilton, T.G., Klinghoffer, R.A., Corrin, P.D., and Soriano, P. (2003). Evolutionary divergence of platelet-derived growth factor alpha receptor signaling mechanisms. *Mol. Cell. Biol.* *23*, 4013–4025.
- Han, M., Yang, X., Farrington, J.E., and Muneoka, K. (2003). Digit regeneration is regulated by *Msx1* and *BMP4* in fetal mice. *Development* *130*, 5123–5132.
- Han, M., Yang, X., Lee, J., Allan, C.H., and Muneoka, K. (2008). Development and regeneration of the neonatal digit tip in mice. *Dev. Biol.* *315*, 125–135.
- Illingworth, C.M. (1974). Trapped fingers and amputated finger tips in children. *J. Pediatr. Surg.* *9*, 853–858.
- Johnston, A.P., Yuzwa, S.A., Carr, M.J., Mahmud, N., Storer, M.A., Krause, M.P., Jones, K., Paul, S., Kaplan, D.R., and Miller, F.D. (2016). Dedifferentiated Schwann cell precursors secreting paracrine factors are required for regeneration of the mammalian digit tip. *Cell Stem Cell* *19*, 433–448.
- Kang, S.H., Fukaya, M., Yang, J.K., Rothstein, J.D., and Bergles, D.E. (2010). NG2+ CNS glial progenitors remain committed to the oligodendrocyte lineage in postnatal life and following neurodegeneration. *Neuron* *68*, 668–681.
- Karamboulas, K., Dranse, H.J., and Underhill, T.M. (2010). Regulation of BMP-dependent chondrogenesis in early limb mesenchyme by TGFbeta signals. *J. Cell Sci.* *123*, 2068–2076.
- Kim, S.W., Pajevic, P.D., Selig, M., Barry, K.J., Yang, J.Y., Shin, C.S., Baek, W.Y., Kim, J.E., and Kronenberg, H.M. (2012). Intermittent parathyroid hormone administration converts quiescent lining cells to active osteoblasts. *J. Bone Miner. Res.* *27*, 2075–2084.
- Korsunsky, I., Millard, N., Fan, J., Slowikowski, K., Zhang, F., Wei, K., Baglaenko, Y., Brenner, M., Loh, P., and Raychaudhuri, S. (2019). Fast, sensitive and accurate integration of single-cell data with Harmony. *Nat. Methods* *16*, 1289–1296.
- Kragl, M., Knapp, D., Nacu, E., Khattak, S., Maden, M., Epperlein, H.H., and Tanaka, E.M. (2009). Cells keep a memory of their tissue origin during axolotl limb regeneration. *Nature* *460*, 60–65.
- Kumar, A., Godwin, J.W., Gates, P.B., Garza-Garcia, A.A., and Brockes, J.P. (2007). Molecular basis for the nerve dependence of limb regeneration in an adult vertebrate. *Science* *318*, 772–777.
- Lehoczy, J.A., Robert, B., and Tabin, C.J. (2011). Mouse digit tip regeneration is mediated by fate-restricted progenitor cells. *Proc. Natl. Acad. Sci. USA* *108*, 20609–20614.
- Lehoczy, J.A., and Tabin, C.J. (2015). *Lgr6* marks nail stem cells and is required for digit tip regeneration. *Proc. Natl. Acad. Sci. USA* *112*, 13249–13254.
- Madisen, L., Zwingman, T.A., Sunkin, S.M., Oh, S.W., Zariwala, H.A., Gu, H., Ng, L.L., Palmiter, R.D., Hawrylycz, M.J., Jones, A.R., et al. (2010). A robust and high-throughput Cre reporting and characterization system for the whole mouse brain. *Nat. Neurosci.* *13*, 133–140.
- Maere, S., Heymans, K., and Kuiper, M. (2005). BiNGO: a Cytoscape plugin to assess overrepresentation of gene ontology categories in biological networks. *Bioinformatics* *21*, 3448–3449.
- Muneoka, K., Fox, W.F., and Bryant, S.V. (1986). Cellular contribution from dermis and cartilage to the regenerating limb blastema in axolotls. *Dev. Biol.* *116*, 256–260.
- Neufeld, D.A., and Zhao, W. (1995). Bone regrowth after digit tip amputation in mice is equivalent in adults and neonates. *Wound Repair Regen.* *3*, 461–466.
- Ovchinnikov, D. (2009). Alcian blue/alizarin red staining of cartilage and bone in mouse. *Cold Spring Harb. Protoc.* *4*, pdb.prot5170.
- Qiu, X., Hill, A., Packer, J., Lin, D., Ma, Y.A., and Trapnell, C. (2017). Single-cell mRNA quantification and differential analysis with Census. *Nat. Methods* *14*, 309–315.
- Reginelli, A.D., Wang, Y.Q., Sassoon, D., and Muneoka, K. (1995). Digit tip regeneration correlates with regions of *Msx1* (Hox 7) expression in fetal and newborn mice. *Development* *121*, 1065–1076.
- Rinkevich, Y., Lindau, P., Ueno, H., Longaker, M.T., and Weissman, I.L. (2011). Germ-layer and lineage-restricted stem/progenitors regenerate the mouse digit tip. *Nature* *476*, 409–413.
- Scialdone, A., Natarajan, K.N., Saraiva, L.R., Proserpio, V., Teichmann, S.A., Stegle, O., Marioni, J.C., and Buettner, F. (2015). Computational assignment of cell-cycle stage from single-cell transcriptome data. *Methods* *85*, 54–61.
- Shannon, P., Markiel, A., Ozier, O., Baliga, N., Wang, J., Ramage, D., Amin, N., Schwikowski, B., and Ideker, T. (2003). Cytoscape: A software environment for integrated models of biomolecular interaction networks. *Genome Res* *13*, 2498–2504.
- Simkin, J., Han, M., Yu, L., Yan, M., and Muneoka, K. (2013). The mouse digit tip: from wound healing to regeneration. *Methods Mol. Biol.* *1037*, 419–435.
- Singh, S.P., Holdway, J.E., and Poss, K.D. (2012). Regeneration of amputated zebrafish fin rays from de novo osteoblasts. *Dev. Cell* *22*, 879–886.
- Sivaraj, K.K., and Adams, R.H. (2016). Blood vessel formation and function in bone. *Development* *143*, 2706–2715.
- Stewart, S., and Stankunas, K. (2012). Limited dedifferentiation provides replacement tissue during zebrafish fin regeneration. *Dev. Biol.* *365*, 339–349.
- Straube, W.L., and Tanaka, E.M. (2006). Reversibility of the differentiated state: regeneration in amphibians. *Artif. Organs* *30*, 743–755.
- Takeo, M., Chou, W.C., Sun, Q., Lee, W., Rabbani, P., Loomis, C., Taketo, M.M., and Ito, M. (2013). Wnt activation in nail epithelium couples nail growth to digit regeneration. *Nature* *499*, 228–232.
- Torreggiani, E., Matthews, B.G., Pejda, S., Matic, I., Horowitz, M.C., Grcevic, D., and Kalajzic, I. (2013). Preosteocytes/osteocytes have the potential to dedifferentiate becoming a source of osteoblasts. *PLoS One* *8*, e75204.
- Trapnell, C., Cacchiarelli, D., Grimsby, J., Pokharel, P., Li, S., Morse, M., Lennon, N.J., Livak, K.J., Mikkelsen, T.S., and Rinn, J.L. (2014). The dynamics and regulators of cell fate decisions are revealed by pseudotemporal ordering of single cells. *Nat. Biotechnol.* *32*, 381–386.
- Tu, S., and Johnson, S.L. (2011). Fate restriction in the growing and regenerating zebrafish fin. *Dev. Cell* *20*, 725–732.
- Wirth, A., Benyó, Z., Lukasova, M., Leutgeb, B., Wettschureck, N., Gorbey, S., Orsy, P., Horváth, B., Maser-Gluth, C., Greiner, E., et al. (2008). G12-G13-LARG-mediated signaling in vascular smooth muscle is required for salt-induced hypertension. *Nat. Med.* *14*, 64–68.
- Wu, S., Wu, Y., and Capecchi, M.R. (2006). Motoneurons and oligodendrocytes are sequentially generated from neural stem cells but do not appear to share common lineage-restricted progenitors in vivo. *Development* *133*, 581–590.
- Wyngaarden, L.A., and Hopyan, S. (2008). Plasticity of proximal-distal cell fate in the mammalian limb bud. *Dev. Biol.* *313*, 225–233.
- Yu, L., Dawson, L.A., Yan, M., Zimmel, K., Lin, Y.L., Dolan, C.P., Han, M., and Muneoka, K. (2019). BMP9 stimulates joint regeneration at digit amputation wounds in mice. *Nat. Commun.* *10*, 424.
- Yu, L., Han, M., Yan, M., Lee, E.C., Lee, J., and Muneoka, K. (2010). BMP signaling induces digit regeneration in neonatal mice. *Development* *137*, 551–559.
- Yuzwa, S.A., Borrett, M.J., Innes, B.T., Voronova, A., Ketela, T., Kaplan, D.R., Bader, G.D., and Miller, F.D. (2017). Developmental emergence of adult neural stem cells as revealed by single-cell transcriptional profiling. *Cell Rep.* *21*, 3970–3986.
- Yuzwa, S.A., Yang, G., Borrett, M.J., Clarke, G., Cancino, G.I., Zahr, S.K., Zandstra, P.W., Kaplan, D.R., and Miller, F.D. (2016). Proneurogenic ligands defined by modeling developing cortex growth factor communication networks. *Neuron* *91*, 988–1004.

## STAR★METHODS

### KEY RESOURCES TABLE

REAGENT or RESOURCE	SOURCE	IDENTIFIER
<b>Antibodies</b>		
Goat polyclonal anti-PDGFR $\alpha$	R & D Systems	Cat#AF1062; RRID: AB_2236897
Rat monoclonal anti-CD31	BioLegend	Cat#102501; RRID: AB_312908
Rabbit polyclonal anti-p75NTR	Promega	Cat#G3231; RRID: AB_430853
Goat polyclonal anti-K14	Santa Cruz Biotechnology	Cat#SC-17104; RRID: AB_10181889
Chicken polyclonal anti-K15	Covance	Cat#PCK-153P; RRID: AB_10067404
Rabbit polyclonal anti-IBA1	Wako	Cat#019-19741; RRID: AB_839504
Goat polyclonal anti-osteocalcin	Bio-Rad	Cat#7060-1815; RRID: AB_2243524
Rat monoclonal anti-THY1	Abcam	Cat#AB3105; RRID: AB_2287350
Rabbit polyclonal anti-ARSI	Novus Biologicals	Cat#NBP1-83678; RRID: AB_11010741
Goat polyclonal anti-ALPL	R & D Systems	Cat#AF2910; RRID: AB_664062
Mouse monoclonal anti-LTBP2	Santa Cruz Biotechnology	Cat#SC-166199; RRID: AB_2265996
Rabbit monoclonal anti-CLEC3B (Tetranectin)	Abcam	Cat#AB108999; RRID: AB_10863748
Rabbit polyclonal anti-SP7	Abcam	Cat#AB22552; RRID: AB_2194492
Rabbit monoclonal anti-CD34	Abcam	Cat#AB198395
Rabbit polyclonal anti-VCAN	Abcam	Cat#AB19345; RRID: AB_444865
Sheep polyclonal anti-DMP1	R & D Systems	Cat#AF4386; RRID: AB_2091367
<b>Biological Samples</b>		
Embryonic limb and postnatal or adult digit tips from C57BL/6 and transgenic mice described in Experimental Models: Organisms and Strains below.	This paper	N/A
Dermal fibroblasts from <i>Pdgfra</i> -CreERT neonatal mice as described in Experimental Models: Organisms and Strains below.	This paper	N/A
<b>Chemicals, Peptides, and Recombinant Proteins</b>		
Tamoxifen	Sigma	Cat#T5648
5-Ethynyl-2'-deoxyuridine	Invitrogen	Cat#E10187
Alizarin Red S	Sigma	Cat#A5533
Alcian Blue 8GX	Sigma	Cat#A3157
Liberase	Millipore Sigma	Cat#5401119001
(Z)-4-Hydroxytamoxifen	Sigma	Cat#H7904
<b>Critical Commercial Assays</b>		
Click-iT Alexa Fluor 647 Imaging Kit	Thermo Fisher	Cat#C10340
RNAscope Fluorescent Multiplex Detection Reagents	ACDBio	Cat#320851
<b>Deposited Data</b>		
scRNA-seq raw datasets from mouse digit tips or limbs processed at the following time points: Uninjured, Uninjured_2, 7DPA, 10 DPA, 14 DPA, 14_2 DPA, 28 DPA and 56 DPA regenerative; E11, E14 and PN3; 10 DPA, 10_2 DPA, 14 DPA non-regenerative; Uninjured and 14 DPA Dmp1CreERT2;TdT	This Paper	GEO: GSE135985
<b>Experimental Models: Organisms/Strains</b>		
C57BL/6	Charles River	Cat#027
NOD.CB17- <i>Prkdc</i> <sup>scid</sup> /NCrCrI	Charles River	Cat#394; RRID: IMSR_CRL:394
B6N.Cg-Tg( <i>Pdgfra</i> -cre/ERT)467Dbe/J	The Jackson Laboratory	Cat# JAX:018280; RRID: IMSR_JAX:018280
B6.129S4- <i>Pdgfra</i> <sup>tm11</sup> (EGFP) <sup>Sor</sup> /J	The Jackson Laboratory	Cat# JAX:007669; RRID: IMSR_JAX:007669
B6.Cg-Tg(Dmp1-cre/ERT2)D77Pdp/J	The Jackson Laboratory	Cat# JAX:029594; RRID: IMSR_JAX:029594

(Continued on next page)

**Continued**

REAGENT or RESOURCE	SOURCE	IDENTIFIER
B6.FVB-Tg(Myh11-cre/ERT2)1Soff/J	The Jackson Laboratory	Cat# JAX:019079; RRID: IMSR_JAX:019079
B6.Cg-Gt(ROSA)26Sor <sup>tm9(CAG-tdTomato)Hze</sup> /J	The Jackson Laboratory	Cat# JAX:007909; RRID: IMSR_JAX:007909
B6;129-Gt(ROSA)26Sor <sup>tm1(DTA)Mrc</sup> /J	The Jackson Laboratory	Cat# JAX:010527; RRID: IMSR_JAX:010527
<b>Software and Algorithms</b>		
Adobe Photoshop CC	Adobe Systems	<a href="https://www.adobe.com/products/photoshop.html">https://www.adobe.com/products/photoshop.html</a> ; RRID:SCR_014199
Adobe Illustrator CC	Adobe Systems	<a href="https://www.adobe.com/products/illustrator.html">https://www.adobe.com/products/illustrator.html</a> ; RRID:SCR_010279
Volocity Image Acquisition Software (Version 6.3)	Perkin Elmer	<a href="https://www.perkinelmer.com/lab-solutions/resources/docs/BRO_VolocityBrochure_PerkinElmer.pdf">https://www.perkinelmer.com/lab-solutions/resources/docs/BRO_VolocityBrochure_PerkinElmer.pdf</a> ; RRID:SCR_002668
Zen Image Acquisition Software (Version 2.3)	Zeiss Microscope	<a href="https://www.zeiss.com/microscopy/int/products/microscope-software/zen.html">https://www.zeiss.com/microscopy/int/products/microscope-software/zen.html</a> ; RRID: SCR_013672
ImageJ	NIH	<a href="https://imagej.nih.gov/ij/">https://imagej.nih.gov/ij/</a> ; RRID:SCR_003070
GraphPad Prism 5	GraphPad	<a href="https://www.graphpad.com/scientific-software/prism/">https://www.graphpad.com/scientific-software/prism/</a> ; RRID:SCR_002798
Seurat R Package (Multiple Versions)	Laboratory of Rahul Satija	<a href="http://satijalab.org/seurat/">http://satijalab.org/seurat/</a> ; RRID:SCR_016341
Cell Ranger Single-Cell Software Suite (Version 3.1)	10X Genomics	<a href="https://support.10xgenomics.com/single-cell-gene-expression/software/pipelines/latest/installation">https://support.10xgenomics.com/single-cell-gene-expression/software/pipelines/latest/installation</a> ; RRID:SCR_016957
RProject for Statistical Computing	R Foundation	<a href="https://www.r-project.org/">https://www.r-project.org/</a> ; RRID:SCR_001905
Cyclone Cell-Cycle Analysis Algorithm	Scialdone et al., 2015	N/A
Monocle (Version 2)	Laboratory of Cole Trapnell	<a href="http://cole-trapnell-lab.github.io/monocle-release/docs/">http://cole-trapnell-lab.github.io/monocle-release/docs/</a>
Biological Networks Gene Ontology Tool (Version 3.0.3)	Maere et al., 2005	<a href="https://www.psb.ugent.be/cbd/papers/BiNGO/Download.html">https://www.psb.ugent.be/cbd/papers/BiNGO/Download.html</a> ; RRID:SCR_005736
Cytoscape (Version 3.4.0)	Shannon et al., 2003	<a href="https://cytoscape.org/">https://cytoscape.org/</a> ; RRID:SCR_015784
Harmony Batch-Effect Correction Algorithm	Korsunsky et al., 2019	N/A
<b>Other</b>		
FISH probe: Mouse <i>Scara5-01</i> (Genbank: NM_028903.2), Channel 1	ACDBio	Cat#522301
FISH probe: Mouse <i>Nrg2</i> (Genbank: NM_001167891.1), Channel 1	ACDBio	Cat#418191
FISH probe: Mouse <i>Sfrp2</i> (Genbank: NM_009144.2), Channel 1	ACDBio	Cat#400381
FISH probe: Mouse <i>Dlx5</i> (Genbank: NM_010056.3), Channel 3	ACDBio	Cat#478151-C3
FISH probe: Mouse <i>Msx2</i> (Genbank: NM_013601.2), Channel 2	ACDBio	Cat#421851-C2
FISH probe: Mouse <i>Lhx9</i> (Genbank: NM_001025565.2), Channel 2	ACDBio	Cat#495431-C2
FISH probe: Mouse <i>Bmp5</i> (Genbank: NM_007555.3), Channel 2	ACDBio	Cat#401241-C2
FISH probe: Mouse <i>Ltbp2</i> (Genbank: NM_013589.3), Channel 1	ACDBio	Cat#400561
FISH probe: Mouse <i>Lrrc17</i> (Genbank: NM_028977.1), Channel 1	ACDBio	Cat#444321
FISH probe: Mouse <i>Arsi</i> (Genbank: NM_001038499.1), Channel 1	ACDBio	Cat#502111
FISH probe: Mouse <i>Col11a1</i> (Genbank: NM_007729.2), Channel 1	ACDBio	Cat#439241

(Continued on next page)

### Continued

REAGENT or RESOURCE	SOURCE	IDENTIFIER
FISH probe: Mouse <i>Fbn2</i> (Genbank: NM_010181.2), Channel 1	ACDBio	Cat#313881
FISH probe: Mouse <i>Grem1</i> (Genbank: NM_011824.4), Channel 1	ACDBio	Cat#314741
FISH probe: Mouse <i>Dmp1</i> (Genbank: NM_016779.2), Channel 1	ACDBio	Cat#441171

### LEAD CONTACT AND MATERIALS AVAILABILITY

Further information and requests for resources and reagents should be directed to and will be fulfilled by the Lead Contact, Freda Miller ([fredam@sickkids.ca](mailto:fredam@sickkids.ca)).

### EXPERIMENTAL MODEL AND SUBJECT DETAILS

#### Mice

All animal use was approved by the Hospital for Sick Children Animal Care Committee, in accordance with the Canadian Council of Animal Care policies. In all cases mice had free access to rodent chow and water in a 12-hour dark-light cycle room. All mice were healthy with no obvious behavioural phenotypes. For all studies, mice of either sex were used and mice were randomly allocated to experimental groups. The ages of mice used for experiments ranged from embryonic day 11 (E11) to adulthood (8–12 weeks old), and the specific end-point ages used for each study are indicated in the figure legends. Wild type C57BL/6 and NOD-SCID mice were purchased from Charles River Laboratories (strain codes: 027 and 394 respectively). *Pdgfra*CreERT (B6.N.Cg-Tg(*Pdgfra*-cre/ERT)467Dbe/J; JAX stock #018280) (Kang et al., 2010), *Pdgfra*<sup>EGFP/+</sup> (B6.129S4-*Pdgfra*<sup>tm11</sup>(EGFP)<sup>Sor</sup>/J; JAX stock #007669) (Hamilton et al., 2003), *Dmp1*CreERT2 (B6.Cg-Tg(*Dmp1*-cre/ERT2)D77Pdp/J; JAX stock #029594) (Kim et al., 2012), *Myh11*CreERT2 (B6.FVB-Tg(*Myh11*-cre/ERT2)1Soff/J; JAX stock #019079) (Wirth et al., 2008); *R26-LSL-TdTomato* (B6.Cg-Gt(ROSA)26Sor<sup>tm9(CAG-tdTomato)Hze</sup>/J; JAX stock #007909) (Madisen et al., 2010) and *R26-LSL-DTA* (B6; 129-Gt(ROSA)26Sor<sup>tm1(DTA)Mrc</sup>/J; JAX stock #010527) (Wu et al., 2006) were obtained from Jackson Laboratories. All mice were bred and genotyped as recommended by Jackson Laboratories.

#### Dermal Fibroblast Cell Cultures

To isolate dermal fibroblasts, the dorsal skin of P1-P2 *Pdgfra*CreERT;*R26-LSL-TdT* mice was separated from the epidermis by incubation with 5mg/mL dispase II (Roche) for 12 h at 4 °C. The dermis was then enzymatically dissociated in a solution of 0.25% collagenase A (Roche) at 37 °C for 30 min. Dermal fibroblasts were washed with medium containing DMEM (Invitrogen), 10% fetal bovine serum (FBS) and 1% penicillin/streptomycin (P/S) and filtered through a 70 μm cell strainer, twice. The cells were pelleted by centrifugation for 5 min at 1500 rpm, washed in medium (as described above) and plated out at 50% confluence. Forty-eight hours after initial plating, the medium was changed, at which point (Z)-4-hydroxy-tamoxifen (Sigma) was added at a final concentration of 1 μM in order to induce recombination and expression of TdT in *Pdgfra*-positive dermal fibroblasts. After 72 hours, the medium containing (Z)-4-hydroxy-tamoxifen (Sigma) was exchanged for fresh medium for a further 24 hours, before releasing the cells using 0.25% Trypsin-EDTA (Thermo Fisher). Cells were then either used for transplant assays or plated onto 12 well plates containing glass coverslips at a density of 100,000 cells per well and cultured until 75% confluence at which time they were used for immunofluorescence assays, as described below.

### METHOD DETAILS

#### Animal Surgeries & Tamoxifen Injections

Digit tip amputation experiments were performed as described previously (Simkin et al., 2013; Johnston et al., 2016) using 8 – 12 week old mice that were anaesthetized and underwent amputation of the distal one third of the terminal phalanges for regenerative amputations and amputation of the distal one third of the second phalangeal element for non-regenerative amputations, of the second through fourth hind limb digits. Mice were given subcutaneous meloxicam (5mg/kg) for analgesia immediately before digit tip amputation surgeries and were housed individually. For experiments involving inducible Cre recombinase mouse strains, tamoxifen (Sigma) was dissolved in a sunflower oil/ethanol mixture (9:1) at 30 mg/ml. Mice were injected intraperitoneally with 3mg/day for four consecutive days. All injected mice were observed daily for any abnormalities.

#### EdU Labelling & Analysis

Mice were injected with 100mg/kg 5-Ethynyl-2'-deoxyuridine (EdU) (Molecular Probes) intraperitoneally 24 hours prior to analysis and tissue was processed as outlined below for immunohistochemistry. EdU was detected using Click-IT Alexa Fluor 647 imaging

kit (Thermo Fisher) as per the manufacturer's instructions. To quantify proliferating cells within the uninjured and regenerating digit tip, digital images of sections immunostained for EdU and the reporter line of interest, were acquired using a 20X objective lens on a Zeiss AxioImager M2 system. Adobe Photoshop software (Adobe Systems) was used to manually outline the region corresponding to the blastema and the percentage of EdU and reporter double-positive cells was determined by manual counting. Three sections per digit were analysed, averaged and this value was considered a single biological replicate. At least 3 separate animals were analysed per condition.

### Dermal Fibroblast Transplant Studies

Digit tip amputation surgeries were performed as described above on adult 8 – 12 week old NOD-SCID mice that were anaesthetized and underwent amputation of the distal one third of the terminal phalanges eliciting a regenerative response or amputation of the distal one third of the second phalangeal element eliciting a non-regenerative response, of the second through fourth hind limb digits. At 6 DPA, mice were anaesthetized and a custom 26 gauge needle fitted to a 10  $\mu$ l 1701 series syringe (Hamilton Company) was used to deliver a cell transplant of tamoxifen-treated *PdgfraCreERT;R26-LSL-TdT* dermal fibroblasts (250,000 cells per digit in 1  $\mu$ l hydrogel comprised of PEG monomer, MOPs buffer and DTT in a 1:1:1 ratio) or vehicle alone into the regenerating digit tip or non-regenerative mesenchymal cap. Mice receiving cell transplants were analyzed 8 or 22 days following injection of the cultured dermal fibroblasts (14 DPA and 28 DPA, respectively).

### Tissue Preparation, Immunostaining & Microscopy

Following dissection, digits were fixed in 4% PFA for 24 h at 4°C, followed by decalcification in 0.5M EDTA at pH 7.0 for 10 - 14 days at room temperature with constant rocking and cryopreserved in 30% sucrose for 24 h. Digits were then snap-frozen in O.C.T. and sectioned sagittally at 14 - 18  $\mu$ m. Sections were washed with PBS for 10 min and blocked using 5% BSA (Jackson ImmunoResearch) containing 0.3% Triton-X-100 (Fisher) in PBS for 1 h at room temperature. Tissue sections were then incubated with primary antibodies diluted in 5% BSA in PBS, overnight at 4°C. Appropriate fluorescently labelled secondary antibodies (1:1000) were used for 1 h at room temperature. For visualization of nuclei, sections were counterstained with Hoechst 33258 (Sigma) for 1 h and slides mounted using PermaFluor mounting medium (Thermo Fisher). For antibodies that required antigen retrieval, tissue sections were washed with PBS for 5 min and immersed in citrate buffer solution containing 0.05% Tween20 (Fisher Scientific) at pH 6.0. Sections were first heated in the microwave for 1.5 min at full power followed by a further 1.5 min at 30% power. Sections were allowed to cool for 30 min in the citrate buffer and blocked using 5% BSA (Jackson ImmunoResearch) in PBS, incubated with primary antibodies overnight at 4°C and fluorescently labelled secondary antibodies (1:1000) for 1 h at room temperature. Counterstaining with Hoechst 33258 (Sigma) was performed to visualize the cell nuclei. For immunostaining of cultured dermal fibroblasts, cells were fixed in 4% PFA for 15 min at room temperature. Dermal fibroblasts were blocked and permeabilized with 5% BSA containing 0.3% Triton-X-100 for 1 h at room temperature, incubated with primary antibodies overnight at 4°C, and fluorescently labelled secondary antibodies (1:1000) for 1 h at room temperature, followed by counterstaining with Hoechst 33258. Digital images were acquired with a Quorum Spinning-Disk confocal microscope system using Velocity acquisition software (Perkin Elmer, Waltham, MA) or for quantification with a Zeiss AxioImager M2 system with an X-Cite 120 LED light source and a C11440 Hamamatsu camera using Zen acquisition software (Thornwood, NY). Images were taken with an optical slice thickness of 0.3 – 1  $\mu$ m and projected Z-stacked images are shown.

### Antibodies

Primary antibodies used were as follows: goat anti-PDGFR $\alpha$  ([1:100]; R & D Systems; cat#AF1062), rat anti-CD31 ([1:250]; BioLegend; cat#102501), rabbit anti-p75NTR ([1:250]; Promega; cat#G3231), goat anti-K14 ([1:250]; Santa Cruz; cat#SC-17104), chicken anti-K15 ([1:250]; Covance cat#PCK-153P), rabbit anti-IBA1 ([1:250]; Wako; cat#019-19741), goat anti-osteocalcin ([1:250]; Bio-Rad; cat#7060-1815; rat anti-THY1 ([1:250]; Abcam; cat#AB3105), rabbit anti-ARSI ([1:250]; Novus Biologicals; cat#NBP1-83678), goat anti-ALPL ([1:250]; R & D Systems; cat#AF2910), mouse anti-LTBP2 ([1:250]; Santa Cruz; cat#SC-166199), rabbit anti-CLEC3B ([1:250]; Abcam; cat#AB108999), rabbit anti-SP7 ([1:250]; Abcam; cat#AB22552), rabbit anti-CD34 ([1:250]; Abcam; cat#AB198395), rabbit anti-VCAN ([1:250]; Abcam; cat#AB19345) and sheep anti-DMP1 ([1:250]; R & D Systems; cat#AF4386). Fluorescently labelled highly cross-absorbed secondary antibodies were purchased from Jackson ImmunoResearch and used at a dilution of 1:1000.

### Fluorescence In Situ Hybridization (FISH)

Single molecule FISH was performed as described in [Yuzwa et al. \(2016\)](#) with probes targeting *Scara5-O1* (NM\_028903.2, cat#522301), *Nrg2* (NM\_001167891.1, cat#418191), *Sfrp2* (NM\_009144.2, cat#400381), *Dlx5* (NM\_010056.3, cat#478151-C3), *Msx2* (NM\_013601.2, cat#421851-C2), *Lhx9* (NM\_001025565.2, cat#495431-C2), *Bmp5* (NM\_007555.3, cat#401241-C2), *Ltbp2* (NM\_013589.3, cat#400561), *Lrrc17* (NM\_028977.1, cat#444321), *Arsi* (NM\_001038499.1, cat#502111), *Col11a1* (NM\_007729.2, cat#439241), *Fbn2* (NM\_010181.2, cat#313881), *Grem1* (NM\_011824.4, cat#314741) and *Dmp1* (NM\_016779.2, cat# 441171) mRNA using the RNAscope kit (Advanced Cell Diagnostics), according to the manufacturer's instructions. Briefly, freshly dissected digits were prepared for FISH as for immunostaining under RNase-free conditions using RNase-free reagents and cryo-sectioned sagittally at 14  $\mu$ m. Sections were washed with ethanol, followed by tissue pre-treatment (1:10 dilution) for 20 min, probe hybridization and signal amplification. Positive staining was identified as red or green punctate dots. Z-stack confocal images were taken with an optical slice thickness of 0.3  $\mu$ m and projected Z-stacked images are shown. The scrambled probe provided with the RNAscope kit was used as a negative control.

### Single-Cell Isolation & 10X Genomics

For single cell isolation of the regenerating or non-regenerative digit tips, adult C57BL/6 (Charles River Laboratories) mice underwent digit tip amputation surgeries as described above, and regenerating digit tips, distal to the original amputation site were collected at 7 (10 mice/60 digits), 10 (8 mice/48 digits), 14 (17 mice/102 digits total in 2 independent experiments), 28 (10 mice/60 digits) or 56 (8 mice/48 digits) days post amputation, or the non-regenerative cap was collected at 10 (17 mice/102 digits total in 2 independent experiments) or 14 (10 mice/60 digits) days post amputation. For single cell profiling of the *Dmp1CreERT2;R26R-LSL-TdT* uninjured (9 mice/54 digits) or regenerating digit (7 mice/42 digits), adult mice were subjected to tamoxifen treatment as described above, amputated or harvested (for the uninjured sample) after 10 additional days and the regenerating digit tips distal to the original amputation site were collected at 14 days post amputation. For single cell isolation from adult uninjured digits (18 mice/108 digits total in 2 independent experiments), the distal one third of the digit tips of C57BL/6 (Charles River Laboratories) mice were collected for one run, while for the second run and the *Dmp1CreERT2;R26R-LSL-TdT* uninjured run, an additional 2-3 mm of tissue proximal to the amputation plane was also collected. For the postnatal day 3 mice (26 mice/156 digits), the distal one third of the hind limb digit tips were collected. For single cell isolation of embryonic limb/digit tips, E11 (6 embryos/12 limbs) and E14 embryos (23 embryos/138 digits) were collected from C57BL/6 timed-pregnant mice (Charles River Laboratories) and cells were isolated from the entire hind limb of E11 embryos or the individual digits of E14 embryonic hind limbs. At least 30,000 cells were isolated for each single-cell experiment. Freshly dissected tissue was digested in Liberase (280 $\mu$ g/ml, Roche) at 37 $^{\circ}$ C for 1 h for non-regenerative, embryonic, early postnatal and regenerating samples collected at 7, 10 and 14 days post amputation or 4 h for adult uninjured or regenerating samples collected at 28 and 56 days post amputation and the second 14 day post amputation regenerative sample, with constant agitation. Cells isolated from the second adult uninjured digit tip sample were digested with 0.25% collagenase, type I (Sigma) for 1 h and a further 3 h with Liberase as described above at 37 $^{\circ}$ C in order to liberate bone-associated cells. Enzymatic digestion was halted by the addition of 10% serum and cells were mechanically dissociated using a small-bore-hole glass pipette. Following dissociation, cells were filtered through a 20 $\mu$ m cell strainer (Miltenyi Biotec) and pelleted by centrifugation at 1000 rpm for 5 min (Eppendorf 5804R). The cell pellet was then washed in 1X Hank's balanced salt solution (1X HBSS) and cells were counted with a haemocytometer and pelleted again by centrifugation at 1000 rpm for 5 min (Eppendorf 5804R). The cell pellet was re-suspended in a solution containing 0.04% bovine serum albumin (BSA) in 1X HBSS at a concentration of 500 – 700 cells/ $\mu$ l. 10X Genomics single cell RNA sequencing, including droplet collection, cDNA amplification and sequencing library preparation, was then carried out at the Princess Margaret Genomics facility (Toronto, ON) or The Hospital for Sick Children Centre for Applied Genomics (Toronto, ON) using the 10X Genomics Chromium system as per the manufacturer's guidelines. The libraries were sequenced on an Illumina NextSeq500 at the Princess Margaret Genomics facility (Toronto, ON) or The Hospital for Sick Children Centre for Applied Genomics (Toronto, ON). FASTQ sequencing reads were processed, aligned to the wild type or custom TdTomato mouse genome (mm10) and converted to digital gene expression matrices using the Cell Ranger count function within the Cell Ranger Single-Cell Software Suite with settings as recommended by the manufacturer (<https://support.10xgenomics.com/single-cell-gene-expression/software/overview/welcome>).

### scRNA-seq Data Analysis

10X Genomics scRNA-seq data was analysed using a previously described computational pipeline (Yuzwa et al., 2017; Carr et al., 2019). Briefly, data was filtered and normalized prior to carrying out principal component analysis. The normalization algorithm corrects for differences in sequencing depth and library size by the use of scaling factors within each cell by pooling random subsets of cells, summing their library sizes, and comparing them with average library size across all cells in the group. This is iteratively performed, and the cell-wise scaling factors can be deconvolved from the set of pool-wise scaling factors. Subsequently, using significant principal components, SNN-Cliq-inspired clustering was performed using the *Seurat* package (v. 1.4.0.16) in R with increasing resolution until the number of differentially expressed genes (calculated by the *Seurat* FindMarkers function,  $p < 0.01$  family-wise error rate, Holm's method) between the most similar clusters reached a minimum of 10 - 30 genes. Each dataset was analysed by choosing the most conservative resolution (detailed below) and resolution parameters were only increased if two cell types/subpopulations of known identity, based on the expression of canonical markers, were not separating into distinct clusters appropriately. Consequently, the number of differentially expressed genes between the most similar clusters for all datasets analysed ranged from 95 to 900 genes. For analysis of the C57BL/6 adult uninjured datasets, cell barcodes from all cells sequenced from two independent experiments were extracted from the raw digital gene expression matrices and merged prior to running through the pipeline resulting in 6731 cells. Clusters were used at a resolution of 1.2 (20 clusters identified with 165 differentially expressed genes between most similar clusters). The average number of genes detected per cell for the first uninjured sample was 1797 (SD  $\pm$ 749) and 1328 (SD  $\pm$ 565) for the second sample, and the average number of transcripts was 5704 (SD  $\pm$ 4184) and 3711 (SD  $\pm$  2633), respectively. For analysis of the regenerative 7 DPA dataset, clusters were used at a resolution of 1.2 (11 clusters identified with 95 differentially expressed genes between most similar clusters). The average number of genes detected per cell was 1134 (SD  $\pm$ 971) and the average number of transcripts was 5085 (SD  $\pm$ 4979). For analysis of the regenerative 10 DPA dataset, clusters were used at resolution 1.2 (11 clusters identified with 140 differentially expressed genes between most similar clusters) and the average number of genes detected per cell was 2764 (SD  $\pm$ 1765) while the average number of transcripts was 15,529 (SD  $\pm$ 11,367). For the 14 DPA datasets, cell barcodes from all cells sequenced from two independent experiments were extracted from the raw digital gene expression matrices and merged prior to running through the pipeline resulting in 1981 cells. Clusters were used at a resolution of 0.8 (14 clusters identified with 135 differentially expressed genes between most similar clusters). The average number of genes detected per cell for

the first 14 DPA sample was 3464 (SD  $\pm$ 1355) and 3378 (SD  $\pm$ 1249) for the second sample, and the average number of transcripts was 14,183 (SD  $\pm$ 8531) and 15,652 (SD  $\pm$ 10,414), respectively. For analysis of the 28 DPA regenerated digit dataset, clusters were used at resolution 0.4 (11 clusters identified with 370 differentially expressed genes between most similar clusters) and the average number of genes detected per cell was 1584 (SD  $\pm$ 1076) while the average number of transcripts was 6363 (SD  $\pm$ 6773). For the 56 DPA regenerated digit dataset, clusters were used at a resolution 0.8 (13 clusters identified with 135 differentially expressed genes between most similar clusters) and the average number of genes detected per cell was 1315 (SD  $\pm$ 1052) while the average number of transcripts was 4668 (SD  $\pm$ 6584). For analysis of the 10 DPA non-regenerative datasets, cell barcodes from all cells sequenced from two independent experiments were extracted from the raw digital gene expression matrices and merged prior to running through the pipeline resulting in 1960 cells. Clusters were used at a resolution of 0.4 (8 clusters identified with 900 differentially expressed genes between most similar clusters). The average number of genes detected per cell for the two 10 DPA non-regenerative samples were 2418 (SD  $\pm$ 1384) and 1681 (SD  $\pm$ 1317), while the average number of transcripts for each of the runs were 11,262 (SD  $\pm$ 9500) and 8007 (SD  $\pm$ 8036), respectively. For the 14 DPA non-regenerative dataset, clusters were used at a resolution of 0.4 (11 clusters identified with 470 differentially expressed genes between most similar clusters) and the average number of genes detected per cell was 1612 (SD  $\pm$ 1419) while the average number of transcripts was 6376 (SD  $\pm$ 8217). To generate the combined uninjured and regenerative mesenchymal dataset (Figures 3A and 3B), cell barcodes from the *Pdgfra*-positive mesenchymal clusters from the 10 DPA, 14 DPA, 14 DPA set 2 and uninjured datasets 1 and 2 were extracted from the raw digital gene expression matrices and merged prior to running through the pipeline resulting in 3126 cells. By running the combined raw transcriptomes through the pipeline together, the datasets were normalized relative to each other as described above. Clusters were used at a resolution of 0.4 (9 clusters identified with 160 differentially expressed genes between most similar clusters). To generate the combined uninjured and regenerative mesenchymal dataset including the 7 DPA time point (Figures 3N and 3O), cell barcodes from the *Pdgfra*-positive mesenchymal clusters from the 7 DPA, 10 DPA, 14 DPA, 14 DPA set 2 and uninjured datasets 1 and 2 were extracted from the raw digital gene expression matrices and merged prior to running through the pipeline resulting in 3227 cells. Clusters were used at a resolution of 0.4 (7 clusters identified with 245 differentially expressed genes between most similar clusters). To generate the combined developmental mesenchymal dataset (Figures 4C and 4D), cell barcodes from the *Pdgfra*-positive mesenchymal clusters from the E11, E14 embryonic limb/digit and P3 developing digit tip individual single cell experiments were extracted from the raw digital gene expression matrices and merged prior to running through the pipeline resulting in 7961 cells. Clusters were used at a resolution of 0.4 (9 clusters identified with 485 differentially expressed genes between most similar clusters). For the E11, E14 embryonic limb/digit and P3 developing digit tip individual single cell experiments (individual tSNE plots not shown), the average numbers of genes detected per cell were 3647 (SD  $\pm$ 926) for the E11, 3297 (SD  $\pm$ 949) for the E14 and 2638 (SD  $\pm$ 945) for the P3 dataset, and the average numbers of transcripts were 14,383 (SD  $\pm$ 7272) for the E11, 12,273 (SD  $\pm$ 6846) for the E14 and 11,063 (SD  $\pm$ 7401) for the P3 dataset, respectively. To generate the combined blastema and P3 mesenchymal dataset (Figure 4J), cell barcodes from the *Pdgfra*-positive mesenchymal clusters from regenerating digit tips at 7 DPA, 10 DPA, 14 DPA and 14 DPA set 2, together with the P3 developing digit tip were extracted from the raw digital gene expression matrices and merged prior to running through the pipeline resulting in 2449 cells. Clusters were used at a resolution of 0.4 (8 clusters identified with 490 differentially expressed genes between most similar clusters). To generate the combined regenerative and non-regenerative mesenchymal dataset (Figures 5E and 5F), cell barcodes from the *Pdgfra*-positive mesenchymal clusters from the 10 DPA, 14 DPA set 1 and 2 regenerative datasets and the *Pdgfra*-positive mesenchymal clusters from the 10 DPA set 1 and 2 and 14 DPA non-regenerative datasets were extracted from the raw digital gene expression matrices and merged prior to running through the pipeline resulting in 1920 cells. Clusters were used at a resolution of 0.4 (7 clusters identified with 450 differentially expressed genes between most similar clusters). For analysis of the uninjured *Dmp1CreERT2;R26R-LSL-TdT* digit tip dataset, clusters were used at resolution 0.8 (10 clusters identified with 380 differentially expressed genes between most similar clusters). The average number of genes detected per cell was 1134 (SD  $\pm$ 971) and the average number of transcripts was 13,698 (SD  $\pm$ 4979). To select the *tdTomato*-positive cells from the uninjured *Dmp1CreERT2;R26R-LSL-TdT* mesenchymal dataset, a cut off of gene expression levels  $>4.75$  was used to account for low levels of ambient RNA detected in the dataset. For analysis of the 14 DPA *Dmp1CreERT2;R26R-LSL-TdT* regenerating digit tip dataset, clusters were used at resolution 0.4 (10 clusters identified with 820 differentially expressed genes between most similar clusters) and the average number of genes detected per cell was 2395 (SD  $\pm$ 1249) and the average number of transcripts was 9984 (SD  $\pm$ 7539). To generate the 14 DPA *Dmp1CreERT2;R26R-LSL-TdT* mesenchymal dataset (Figure 7A), cell barcodes from the *Pdgfra*-positive mesenchymal cells from the 14 DPA *Dmp1CreERT2;R26R-LSL-TdT* data set were extracted from the raw digit gene expression matrix and processed through the pipeline resulting in 2081 cells. Clusters were used at a resolution of 0.4 (7 clusters identified with 165 differentially expressed genes between most similar clusters). To select the *tdTomato*-positive cells from the 14 DPA *Dmp1CreERT2;R26R-LSL-TdT* mesenchymal dataset, a cut off of gene expression levels  $>2$  was used to account for low levels of ambient RNA detected in the dataset. t-SNE projections, cell-cycle annotations and hierarchical clustering were produced in R using a custom designed Shiny script. t-SNE gene expression overlays displayed in the figures were generated using the FeaturePlot function in *Seurat* while violin plots were generated using the VlnPlot function in R. Dataset identities were distinguished by using the gg colour hue and hcl functions in R. Cell cycle scores were computed using Cyclone analysis as described previously (Scialdone et al., 2015). Correlation analysis comparing gene expression between different clusters or *tdTomato*-positive and negative cells, was performed by averaging the expression of each gene across all cells in individual clusters or categories and then performing Pearson or Spearman correlation analysis using the *cor.test* function in R. To generate UMAP projections (Figures S3D and S5B), the merged digital expression matrix of each dataset was imported into R V3.6.1 and a *Seurat* (V3.1.1) object was created. Data was subsequently filtered for low-expressing cells (min. cell cut off = 3 and

minimum feature count = 200), doublets (> twice the mean expression) and for cells with high mitochondrial gene expression (<10%). The top 2000 variable features were identified using the vst method and used to run the PCA on scaled data. The UMAP dimensional reduction algorithm was then performed using the top 20 PC in R.

Clusters or cell types were identified based on the expression of the following marker genes (amongst others) as Schwann lineage cells - *Sox10* (SRY-box transcription factor 10), *Sox2* (SRY box transcription factor 2) and *Plp1* (Proteolipid protein 1); endothelial cells - *Pecam1* (Platelet and endothelial cell adhesion molecule 1), *Tie1* (Tyrosine kinase with immunoglobulin like and EGF like domains 1) and *Cdh5* (Cadherin 5); vascular smooth muscle/pericytes - *Myh11* (Myosin heavy chain 11), *Rgs5* (Regulator of G protein signalling 5), *Mylk* (Myosin light chain kinase) and *Pdgfrb* (Platelet derived growth factor receptor beta); mesenchymal cells: *Pdgfra* (Platelet derived growth factor receptor alpha), *Pdgfrb* (Platelet derived growth factor receptor beta) and *Prrx2* (Paired related homeobox 2); immune cells/macrophages - *Aif1* (Allograft inflammatory factor 1), *Tnfrsf11a* (TNF receptor superfamily member 11a) and *Tnfrsf13b* (TNF receptor superfamily member 13B); epithelial cells - *Krt5* (Keratin 5), *Krt14* (Keratin 14) and *Krt10* (Keratin 10). To quantify the percentage of cells from each of the individual 14 DPA and replicate 14 DPA datasets, the number of cells in a given cell type as defined by the expression of cell-type specific marker genes listed above, were quantified and divided by the total number of cells for that particular dataset in R.

Differential correlation of single cell transcriptomes with P3 developing mesenchymal digit tip versus mature mesenchymal uninjured digit tip and 7 DPA, 10 DPA and 14 DPA regenerating digit tip mesenchymal transcriptomes were calculated as described previously (Gerber et al., 2018). Briefly, mock bulk transcriptomes were generated for each time point by taking the mean expression of each gene for all cells of a given time point. Each single-cell transcriptome was subsequently correlated with each of the mock bulk transcriptomes. For each cell, we subtracted the correlation of its transcriptome with the P3 developing mesenchymal transcriptome, from the correlation of its transcriptomes with the uninjured adult mesenchymal transcriptomes (y-axis). In a similar manner, the differential correlation with the 14 DPA blastema (late blastema), versus the average of the combined 7 DPA and 10 DPA (early blastema), were generated (x-axis).

Single-cell pseudo-time trajectories were constructed using Monocle 2 as previously described (Trapnell et al., 2014; Qiu et al., 2017) with the following modifications. Briefly, cell barcodes from the *Pdgfra*-positive mesenchymal clusters from the desired datasets (Figures 3P and S3P– 7, 10, 14, 14 DPA set 2 regenerative and uninjured 1 and 2 datasets; Figures 4A and 4C – 7, 10, 14, 14 DPA set 2 regenerative, 28, 56 DPA regenerated and uninjured 1 and 2 datasets; Figures 4G, 4H, and S4F – 7, 10, 14, 14 DPA set 2 regenerative, uninjured 1 and 2 datasets as well as E11, E14 and P3 developing datasets; Figures 5H and S5G – 10, 14, 14 DPA set 2 regenerative or 10 DPA set 1 and 2, 14 DPA non-regenerative in combination with uninjured 1 and 2, E11, E14 and P3 datasets) were extracted from the raw digital gene expression matrices and merged prior to normalization using Monocle's size factor normalization method. We then performed principal component analysis using the same highly variable genes that were obtained from our custom built pipeline as described above and the cells were projected into 2-dimensional space using the t-SNE algorithm. Cells were subsequently assigned into distinct clusters using Monocle's density peak clustering algorithm. A set of ordering genes was collected by testing each gene for differential expression between the clusters in the dataset and selecting the top 1000 significantly differentially expressed genes. Expression profiles were subsequently reduced to 2 dimensions using the DDRTree algorithm included in Monocle 2 and cells were ordered using these 1000 differentially expressed genes to obtain a trajectory. The set of ordering genes was determined for each of the merged datasets, excluding those genes not detected in at least 10 cells.

Batch correction was performed using the Harmony batch-effect-correction method (Korsunsky et al., 2019) with Seurat V2. Briefly, normalized gene expression data was imported into Seurat where highly variable genes were used to carry out PCA. Subsequently, PCA embeddings were corrected for batch differences using the HarmonyMatrix function. t-SNE dimensionality reduction was then performed on the top 20 harmonized PCs to project cells into two dimensional space.

### Identification of Transcriptional Signatures

The *VennDiagram* package in R was used to directly compare mRNAs that were differentially up-regulated in the 10 DPA, 14 DPA (datasets 1 and 2) and uninjured (datasets 1 and 2) *Pdgfra*-positive clusters relative to the total cell datasets at each time point ( $p < 0.01$ , FWER) (Figure S3E; Table S1). For table classification, t-SNE overlays were visualized individually to accurately select genes expressed as indicated in the Supplemental Tables. For blastema signature genes, the 1541 genes (Table S1) enriched in the 10 and/or 14 DPA blastema datasets were analyzed and categorized as follows: (i) those genes expressed in  $\geq 10\%$  of 10 DPA and/or 14 DPA and in  $\leq 4\%$  of 1993 cells in the uninjured digit tip *Pdgfra*-positive mesenchymal cells and (ii) those genes expressed in  $\geq 10$ -fold of 10 DPA and/or 14 DPA and in 4-10% of uninjured digit tip *Pdgfra*-positive mesenchymal cells (Table S2). For regeneration-enriched genes, we analyzed the 1480 genes (Table S4) enriched in 10 DPA and 14 DPA regenerative versus non-regenerative *Pdgfra*-positive clusters. We selected those genes that were expressed in  $\leq 10\%$  of non-regenerative cells and in  $\geq 2$ -fold more regenerative cells (Table S5). Genes associated with proliferation were excluded in both cases.

### Gene Ontology Analysis

The Biological Networks Gene Ontology tool (BiNGO, version 3.0.3) was used to determine which Gene Ontology (GO) terms were significantly overrepresented for the 123 regeneration-enriched genes ( $p < 0.001$ ). Molecular interaction networks were visualized using Cytoscape (version 3.4.0). A hypergeometric test with Benjamini and Hochberg False Discovery Rate (FDR) correction (Benjamini, and Hochberg, 1995) at a significance level of at least 0.001 was used. Corrected p-values were calculated using a  $-\log_{10}$  conversion. A balloon plot was generated in R using the *ggballoonplot* function within the *ggplot2*-based package *ggpub2* 0.2.

## QUANTIFICATION AND STATISTICAL ANALYSIS

### Morphometric Analyses of Bones & Nails

To quantify nail length and area, digital images of freshly dissected nails were taken on a Leica fluorescence stereomicroscope (Buffalo Grove, IL) equipped with a Micropublisher 5.0 RTV colour camera and a Plan-Apo 1X objective lens, operated by Volocity acquisition software. ImageJ analysis software (Bethesda, MD) was used to trace outlines of the regenerated nails and to measure length and area in a blinded manner. For bone analysis, digits were subjected to whole-mount skeletal staining as previously described (Ovchinnikov, 2009). Briefly, digits were placed in 1M NaCl at room temperature for 12 – 24 h to facilitate removal of cutaneous tissues and nail, then dehydrated in 95% ethanol for 24 h prior to staining in 0.03% Alcian Blue 8GX solution (Sigma) for a further 24 h. Digits were then washed in 95% ethanol and stained for 4 h in 0.03% Alizarin Red S (Sigma) before clearing for 5 – 7 days in a 20% glycerol/1% KOH solution. The regenerated phalanges were imaged and quantified as described above for nail quantification. For both nail and bone quantification, each digit was considered as a single biological replicate. At least 3 separate mice were utilized in each experimental condition.

### Quantification of Reporter-Positive Cells

Uninjured and regenerating digit tips of adult *PdgfraCreERT;R26-LSL-TdT* and regenerating digit tips of adult *Pdgfra<sup>EGFP/+</sup>* or *Dmp1CreERT2;R26-LSL-TdT* mice were analyzed at 14 DPA for the TdT or EGFP reporters and counterstained with Hoechst 33258 (Sigma). Stitched images were acquired on a Zeiss AxioImager M2 system equipped with an X-cite 120 LED light source and a C11440 Hamamatsu camera. The uninjured distal digit tip or the regenerated region, exclusive of the epithelium/nail, was outlined and the proportion of reporter-positive cells per section/Hoechst-positive cells was manually counted using Adobe Photoshop software (Adobe Systems Incorporated). Two sections per uninjured digit tip and three sections per regenerating digit were analyzed, and these counts were averaged and considered as a single biological replicate. A minimum of at least 3 separate animals were analysed per condition.

### Quantification of PDGFR $\alpha$ + Cells & Section Area

Adult *PdgfraCreERT-R26-LSL-DTA* mice and *R26-LSL-DTA* control mice were administered tamoxifen (as described above) for 4 days and either collected 10 days later or amputated and collected 14 or 28 days later, immunostained for PDGFR $\alpha$  and counterstained with Hoechst 33258 (Sigma). Stitched images were acquired on a Zeiss AxioImager M2 system and all quantification was performed in a blinded manner. In uninjured digit tips, the proportion of PDGFR $\alpha$ -positive/Hoechst-positive cells located distal to the predicted plane of amputation were manually counted using Adobe Photoshop software (Adobe Systems Incorporated). In 14 DPA digits, the regenerating region, exclusive of the epithelium/nail, was outlined and the proportion of PDGFR $\alpha$ -positive cells/Hoechst-positive cells was manually counted using Adobe Photoshop software (Adobe Systems Incorporated). To quantify section area, digits from 14 DPA and 28 DPA *PdgfraCreERT-R26-LSL-DTA* mice, *R26-LSL-DTA* tamoxifen-treated control mice and adult uninjured C57BL/6 mice were sectioned and counterstained with Hoechst 33258 (Sigma). Stitched images were acquired on a Zeiss AxioImager M2 system and ImageJ analysis software (Bethesda, MD) was used to trace outlines of the uninjured and regenerated region, exclusive of the epithelium/nail and measure section area. Two sections per uninjured digit tip and three sections per regenerating/regenerated (14 & 28 DPA ablated and control mice) digit tip were analyzed and these counts were averaged and considered a single biological replicate. A minimum of at least 3 separate animals were analysed per condition.

### Quantification of *Dmp1CreERT2-TdT+* Bone Lacunae

Uninjured or regenerated digit tips at 28 DPA from *Dmp1CreERT2;R26-LSL-TdT* were sectioned and analyzed by immunostaining for osteocalcin (OCN) in order to mark the mineralized bone matrix and osteocyte-containing lacunae of the terminal phalangeal element. Sections were also counterstained with Hoechst 33258 (Sigma) prior to acquisition of fluorescence images using a Zeiss AxioImager M2 system. In the uninjured digit tips, the proportion of TdT-positive lacunae /Hoechst-positive lacunae located distal to the predicted plane of amputation were manually counted using Adobe Photoshop software (Adobe Systems Incorporated). In the 28 DPA regenerated digit tips, the proportion of TdT-positive lacunae/Hoechst-positive lacunae located distal or proximal to the actual plane of amputation were counted. Two sections per digit were analyzed and these counts were averaged and considered a single biological replicate. A minimum of at least 3 separate animals were analysed per condition.

### Quantification of *Dmp1CreERT2-TdT+* Cells in Vessels

Uninjured digit tips from *Dmp1CreERT2;R26-LSL-TdT* were sectioned and analyzed by immunostaining for CD31 in order to mark vasculature. Sections were also counterstained with Hoechst 33258 (Sigma) prior to acquisition of stitched fluorescence images using a Zeiss AxioImager M2 system. In the uninjured digit tips, the proportion of TdT-positive/Hoechst-positive cells located in the mineralized bone matrix of the terminal phalanx associated with CD31-positive vasculature was manually counted using Adobe Photoshop software (Adobe Systems Incorporated). Three sections per digit were analyzed and these counts were averaged and considered a single biological replicate. A minimum of at least 3 separate animals were analyzed.

### Statistical Testing of Populations in scRNA-Seq Data

To test if cells within two different populations were statistically different, a 'signature' for the population of interest was generated by selecting the top 100 differentially expressed genes (calculated by the Seurat FindMarkers function,  $p < 0.01$  FWER, Holm's method) between groups. Scoring was performed by summing the expression values of the 'signature' genes for each cell in both populations and scores were subsequently compared by performing a Wilcoxon signed-rank test in R.

### Quantification of Monocle Trajectories

To quantify the percentage of cells from individual datasets, the numbers of cells in a given state were extracted from the Monocle 2 program (Figures 3P, 4A, S3P, and S4C) and divided by the total number of cells for that particular dataset.

### Quantification of Blastema Genes during Regeneration

To calculate the proportion of cells expressing the blastema transcriptional signature genes during long term regeneration relative to its peak level in the blastema (Figure 4B), we determined the difference between the proportion of positive uninjured cells versus the proportion of 10 or 14 DPA cells (whichever was highest;  $\Delta y$ ) and the proportion of uninjured cells versus 28 or 56 DPA cells ( $\Delta x$ ). We expressed  $\Delta x/\Delta y$  as a percentage score indicating where a gene's expression at 28 or 56 DPA was along the trajectory from uninjured (lowest) to blastema (peak levels). Genes were then categorized into the following bins based on this trajectory score: 1 - Baseline (similar to the levels in the uninjured mesenchymal cells), 2 -  $\leq 10\%$  of the peak values normalized to the baseline, 3 - 11-20%, 4 - 21-30%, 5 - 31-40%, 6 - 41-50% and 7 -  $\geq 51\%$ . A similar analysis was used to compare expression of the blastema signature genes in the non-regenerative mesenchymal cells.

### Statistical Analysis

With the exception of the scRNA-seq analyses, statistical significance was determined using a two-tailed Student's t-test with  $p < 0.05$  considered to be statistically significant. Error bars indicated the standard error of the mean (S.E.M.). Statistics used for the computational analyses are described in the relevant sections.

### DATA AND CODE AVAILABILITY

The raw scRNA-seq datasets have been deposited in the GEO database under the ID code GEO: GSE135985.